Asian Journal of Civil Engineering (2025) 26:2475–2497
https://doi.org/10.1007/s42107-025-01323-w

RESEARCH

Seismic response prediction of asymmetric structures with SMA dampers using machine learning algorithms

Anant Parghi[1] · Jay Gohel[1] · Apurwa Rastogi[1] · Melda Yucel[2] · Cigdem Avci-Karatas[3] · Snehal Mevada[4]

Received: 11 March 2025 / Accepted: 25 March 2025 / Published online: 21 April 2025

Abstract

The dynamic response of asymmetric structures to seismic forces is challenging due to mass, stiffness, and damping distribution irregularities. Shape memory alloy (SMA) dampers have successfully dealt with these issues because of their distinctive super elasticity and energy dissipation characteristics. In this work, we study regression algorithms' effectiveness in predicting the seismic behavior of asymmetric structures installed with SMA dampers. A numerical simulation produces a comprehensive dataset of structural parameters consisting of the structure's varying periods, frequency ratios, and eccentricity ratios. The critical responses of structures, including lateral and torsional displacement, lateral and torsional acceleration, and stiff and flexible edge damper forces, are predicted using machine learning (ML) techniques, artificial neural networks, decision trees, support vector machines, ensemble bagged trees, and Gaussian process regression. The model is validated using performance metrics such as mean absolute error and root mean square error, mean absolute percentage error, coefficient of determination, and Shapley Additive explanations values, ensuring that predictions are robust and consistent. The results revealed that regression methods accurately model the nonlinear dynamic behavior of SMA dampers in asymmetric structures, providing exact and computationally efficient predictions of seismic response. This predictive paradigm facilitates optimal damper configuration, minimizing the computational complexity of iterative design methods. The proposed research integrates advanced materials with ML methods to create seismically resilient structural systems.

Keywords Shape memory alloys · Asymmetric structure · Advanced materials · Structural eccentricity · Seismic response prediction · Machine learning · Regression algorithms

Introduction

The seismic response of torsionally coupled systems has emerged as an essential component of research worldwide. Torsional irregularities in structures arise from uneven distributions of mass and stiffness, making these structures more susceptible to damage during significant seismic events (Wang et al., 2023). Consequently, it is essential to employ advanced technologies to control the coupled translational-torsional vibrations in asymmetric structures (Chowdhury, 2021; Shyamsunder et al., 2021).

Among various vibration control techniques, seismic dampers have been considered an effective solution for safeguarding structures against major earthquakes (Mevada & Jangid, 2015). Using shape memory alloys (SMA) in vibration control devices represents a cutting-edge focus within the research community (Mohammadgholipour & Billah, 2023; Muntasir Billah et al., 2022; Tabrizikahou et al., 2022). SMA has unique properties like super elasticity and

The original online version of this article was revised: there were errors in figure 4 and 7.

✉ Anant Parghi
amp@amd.svnit.ac.in

[1] Department of Civil Engineering, Sardar Vallabhbhai National Institute of Technology, Surat, Gujarat 395007, India

[2] Department of Civil Engineering, İstanbul Aydin University, 34295, Küçükçekmece, Istanbul, Turkey

[3] Department of Transportation Engineering, Faculty of Engineering, Yalova University, Yalova 77200, Turkey

[4] Structural Engineering Department, B.V.M. Engineering College, Anand (Vallabh-Vidyanagar), Gujarat, India

shape memory effect. Super elastic SMA can almost regain strain (8%) to its original shape after unloading (Zhang et al., 2020a). Moreover, SMA possesses a considerable energy dissipation capacity. Thus, numerous types of dampers have been proposed by many researchers (Falahian et al., 2021; Qian et al., 2016; 2013; Zhang et al., 2020b; Zuo et al., 2008). Recent studies, including Wei et al. (2025), have shown that SMA-high damping rubber dampers can significantly reduce peak inter-story drift and residual displacements in steel frames subjected to primary shock-after-shock sequences, compared to traditional damping systems. Based on the existing research, it is shown that the SMA-based dampers could effectively reduce the response of the structure during seismic events (Falahian et al., 2021; Qian et al., 2013; Zhang et al., 2020b; Zuo et al., 2008).

Machine learning (ML) methodologies in civil engineering have transformed field practices, especially in evaluating infrastructure under diverse conditions (Feng et al., 2020; Kaveh, 2024; Yucel et al., 2019). Kaveh and Zakian (2013, 2014) explored seismic optimization of steel and reinforced concrete (RC) structures, employing meta-heuristic algorithms such as Charged System Search (CSS) to enhance design efficiency. Their studies demonstrated that optimizing steel frames, RC moment frames, and dual shear wall-frame structures under seismic loading can significantly reduce structural weight and cost while satisfying seismic constraints from ACI and FEMA guidelines. Kaveh and Biabani Hamedani (2022) introduced an Improved Arithmetic Optimization Algorithm (IAOA) to address the limitations of traditional Arithmetic Optimization Algorithms (AOA), improving convergence and exploration in discrete structural optimization. Kaveh et al. conducted a statistical seismic performance assessment of the Tuned Mass Damper Inerter (TMDI), demonstrating its effectiveness in mitigating structural vibrations under seismic loads. Their study highlights the integration of an inerter with a traditional TMD system, enhancing energy dissipation and improving seismic resilience (Kaveh et al., 2020). Ghosh et al. (2013) employed surrogate modeling techniques, such as multivariate adaptive regression splines and support vector machine (SVM), to study the seismic behavior of multi-span supported concrete girder bridges. They found that multivariate adaptive

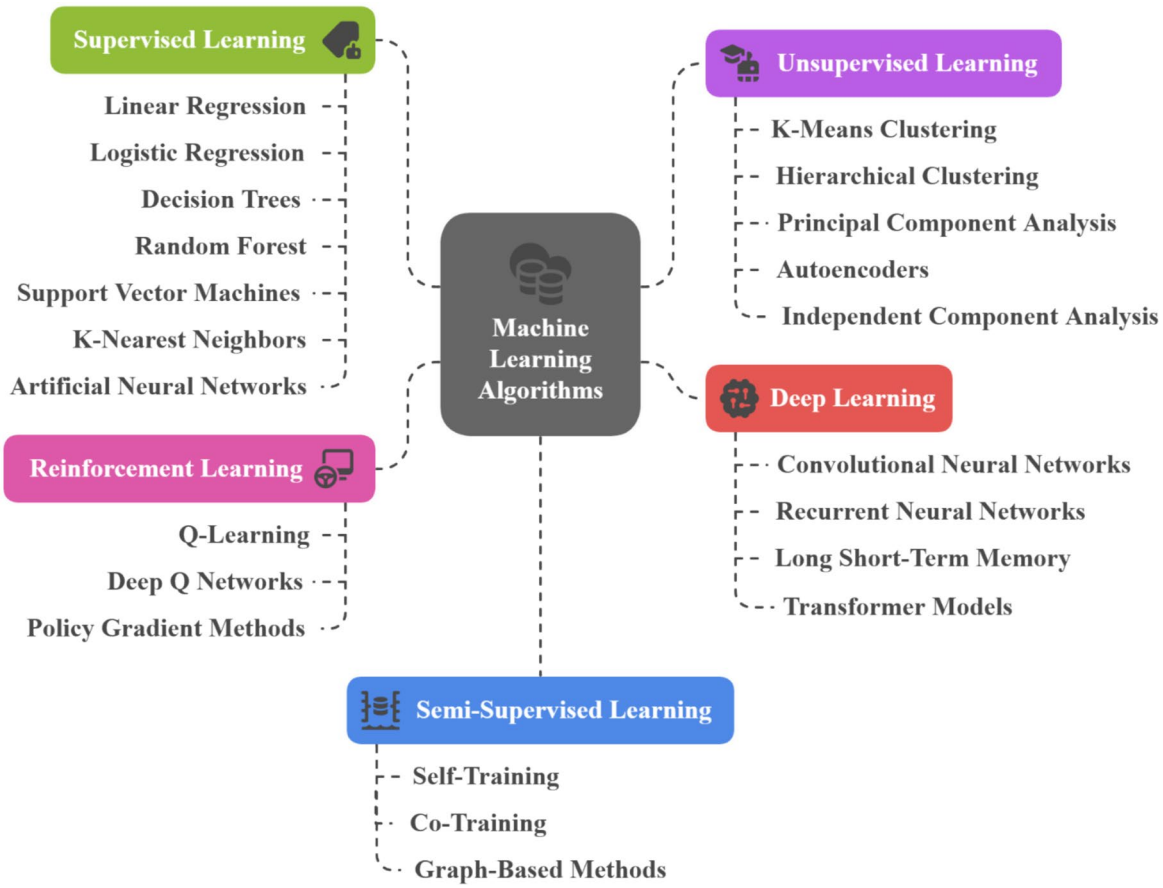

Fig. 1 Machine learning algorithm and their classification

regression splines provided the most accurate predictions with minimal errors, while SVM prediction underperformed.

Figure 1 presents a classification of machine learning techniques into five primary categories. Each method follows a distinct learning approach—Supervised Learning relies on labeled data, while Unsupervised Learning identifies patterns in unlabelled datasets. Reinforcement Learning optimizes decision-making through reward-based interactions, whereas Semi-Supervised Learning leverages labeled and unlabelled data for training. Deep Learning, a subset of machine learning, employs artificial neural networks for complex data representations. This classification is a foundation for selecting appropriate algorithms based on problem-specific requirements (Kaveh, 2024).

Pang et al. (2014) studied the seismic fragility of RC highway bridges using the artificial neural network (ANN) method employing uniform design to select training datasets. Their results demonstrated that the ANN approach significantly reduced computational costs while maintaining accuracy in fragility curve estimations compared to traditional methods. Mahmoudi and Chouinard (2016) applied probabilistic ML techniques, specifically SVM, to assess the seismic vulnerability of highway bridges. Their approach proved more computationally efficient than conventional element-based methods while still delivering reliable estimates of fragility curves. Yang et al. (2023) highlighted the significant influence of pulse-like ground motions on seismic fragility, proposing an ANN-based probabilistic seismic demand model to reduce biases associated with pulse period variations. Their approach improved accuracy in predicting structural responses by incorporating intensity measures such as pulse period ratios. It provided a refined fragility and risk assessment method in near-field earthquake scenarios. Angarita et al. (2024) applied random forest (RF) and ANN models to predict the pushover curves of low-rise reinforced concrete frames, achieving high accuracy with significantly reduced computational costs compared to traditional nonlinear modeling. Similarly, Jia et al. (2025) introduced a deep learning model (FRSNet) to generate floor response spectra, demonstrating superior accuracy and efficiency on single-degree-of-freedom and multi-degree-of-freedom models. Integrating deep learning and ML approaches in seismic performance prediction represents a promising direction and results for efficient and accurate assessment, particularly for structural and non-structural components (Jia et al., 2025).

Based on previous literature, the proposed research aims to develop a regression-based ML technique to predict and assess the effectiveness of SMA dampers in asymmetric buildings under synthetic ground motion. The asymmetric buildings are more vulnerable to damage because of the uneven distribution of mass and stiffness, and there is room for further study. Traditional analytical methods for evaluating the seismic performance of dampers in such structures can be time-consuming and computationally expensive. Therefore, there is a strong need for innovative approaches that can efficiently predict the performance of damping systems in complex structural configurations.

SMA dampers, which exhibit superelastic properties and the ability to undergo excessive deformations while recovering their parent phase, have shown promising results in enhancing the seismic resilience of structures. However, the effectiveness of these dampers in asymmetric buildings, which are prone to torsional responses under seismic loading, requires further investigation. In this research, we use ML techniques to develop predictive models for the performance of SMA dampers, thereby providing a more efficient and accurate means of assessing their effectiveness. We use the asymmetric frame and SMA constitutive model based on the approach explained by Parghi et al. (2024). We considered the time period of the structures (T_y), frequency ratio (ω), and eccentricity ratio (e_x/l) as crucial predictors and predicted the structural response using various ML methods. Moreover, the SHapley Additive exPlanations (SHAP) approach is implemented to find the influences of different structural parameters on the effectiveness of the SMA wire dampers. The SHAP method helps understand the contribution of each input parameter. It provides insights into the factors significantly impacting damping performance, enabling better design and optimization of SMA-based damping systems for seismic applications.

Proposed research methodology

This research methodology entails a comprehensive nonlinear analysis of asymmetric structural frames subjected to seismic loads. The process begins with generating synthetic ground motion, which is subsequently scaled to align with the target response spectrum, ensuring compatibility with the desired seismic conditions. This scaled ground motion is utilized for time history analysis to simulate realistic seismic scenarios. The methodology is illustrated schematically in Fig. 2, clearly representing the steps involved in the research workflow. In the first stage, we prepare the data and conduct nonlinear time history analyses on an asymmetric frame under seismic loading. These analyses yield critical input and output parameters, which form the foundation for subsequent machine learning (ML) applications.

We employ regression algorithms in the ML phase to develop predictive models. The available numerical data is split into two subsets to ensure robust model training and validation: 70% is used for training the models. In contrast, the remaining 30% is reserved for testing and validation. This division allows the model to generalize the unseen data effectively. The methodology includes

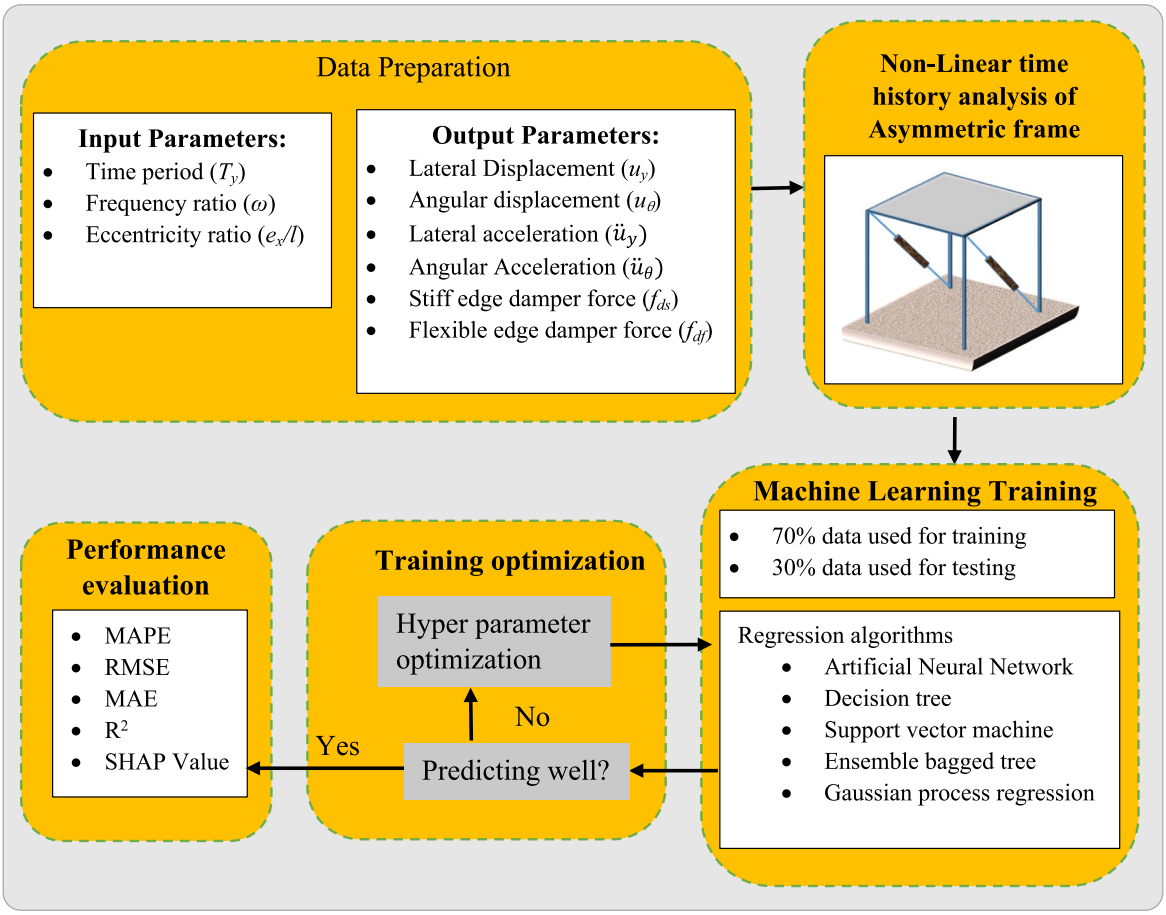

Fig. 2 Flowchart of the proposed research

hyperparameter optimization as a key component to enhance the performance of the ML models. We adjust the models to maximize their predictive accuracy by fine-tuning parameters such as learning rates, regularisation terms, and tree depths. A set of metrics, such as mean absolute percentage error (MAPE), root mean squared error (RMSE), mean absolute error (MAE), and the coefficient of determination (R^2), are used to check how well the trained models work carefully. Additionally, SHAP values are used to interpret the contribution of individual input features to the model's predictions, offering more profound insights into relationships between parameters and outcomes. This structured methodology ensures a systematic approach to analyzing the nonlinear seismic behavior of asymmetric frames while leveraging advanced ML techniques to predict and interpret structural responses accurately.

Numerical model of SMA wire damper

In this research, we employed SMA wire dampers for numerical simulation, validated in a previous study by Parghi et al. (2024). Several parts make up the SMA damper. These are the outer case, the piston rod that moves in two directions, the pre-stressed nitinol wires, the adjustable pre-strain plates with bolts, and the connecting fittings. The damper is attached to the structure through these connecting fittings. The piston rod moves forward and backward in response to the structure's motion. The damper's left side wires are subjected to tension when the rod moves forward, as illustrated in Fig. 3. Conversely, the wires on the right-side experience tensile forces during backward movement. The numerical model developed by Graesser and Cozzarelli (1991) is used to simulate the damper, represented by the following Eq. (1):

$$\dot{\sigma} = E\left[\dot{\epsilon} - |\dot{\epsilon}|\left(\frac{\sigma - \beta}{Y}\right)^n\right] \tag{1}$$

In this formulation, σ denotes the uniaxial stress, ϵ represents the uniaxial strain, and E corresponds to the modulus of elasticity. The terms β and Y signify the kinematic hardening parameter (back-stress) and yield strength, respectively. The constant n regulates the transition

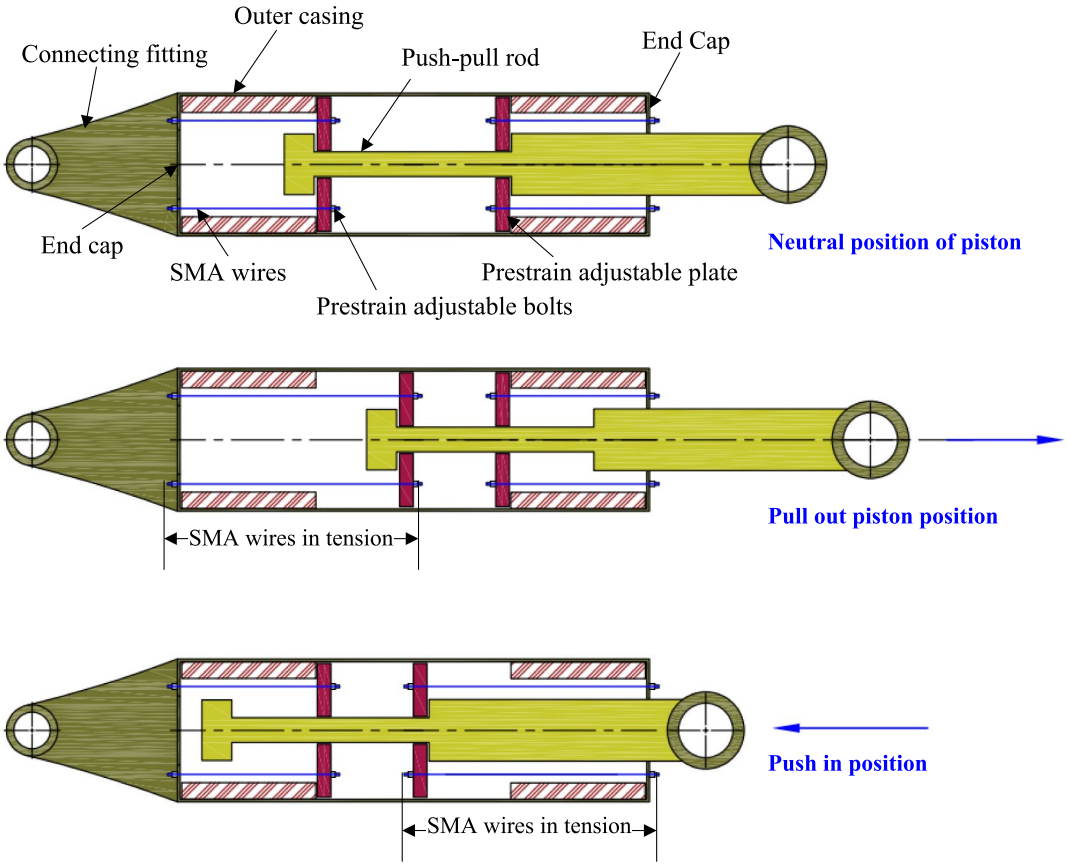

Fig. 3 Schematic diagram of the proposed SMA wire damper (Parghi et al., 2024)

gradient from the elastic regime to the plastic deformation state and is defined as any positive odd real integer. The following relation shown in Eq. (2) expresses the kinematic hardening parameter β:

$$\beta = E\alpha\{\varepsilon_{in} + f_T|\varepsilon|^c erf(a\varepsilon)[u(-\varepsilon\dot{\varepsilon})]\} \tag{2}$$

here f_T, a, and c are material-specific parameters. When $f_T = 0$, the model represents a fully martensitic state. Conversely, for $f_T > 0$, the model exhibits superelastic behavior. The parameter α controls the gradient of the σ—ε response curve and is defined as $\alpha = E_y/(E - E_y)$, where E_y is the tangent modulus in the inelastic region of the σ—ε curve.

Structural modeling

The system under study is an idealized single-story structure featuring columns with varying cross sections and a uniform slab, as illustrated in Fig. 4. The variation in column cross-sections introduces asymmetry into the structure. The slab is assumed to have a uniformly distributed mass, ensuring that its geometric center coincides with its center of mass (C.M.). The seismic excitation is applied to the structure along the *y*-direction. The governing equation of motion for this structural configuration is expressed as Eq. (3) (Kaveh et al., 2015; Parghi et al., 2024):

$$M\ddot{u} + C\dot{u} + Ku = -M\lambda\ddot{u}_g + Df(SMA) \tag{3}$$

M, C, and K represent the mass, damping, and stiffness matrices, respectively. The term λ refers to the influence coefficient vector, while D is a matrix characterizing the placement of the SMA damper. The vector $f(SMA)$ represents the force exerted by the SMA. The term $\ddot{u}_g$ is the vector denoting earthquake ground motion. Given the structural symmetry in the *x*-direction, the analysis considers two degrees of freedom, namely u_y (lateral displacement in the *y*-direction) and u_θ (rotational displacement). The M and K matrices can be expressed as Eqs. (4) and (5), respectively,

$$M = \begin{bmatrix} m & 0 \\ 0 & ml^2 \end{bmatrix} \tag{4}$$

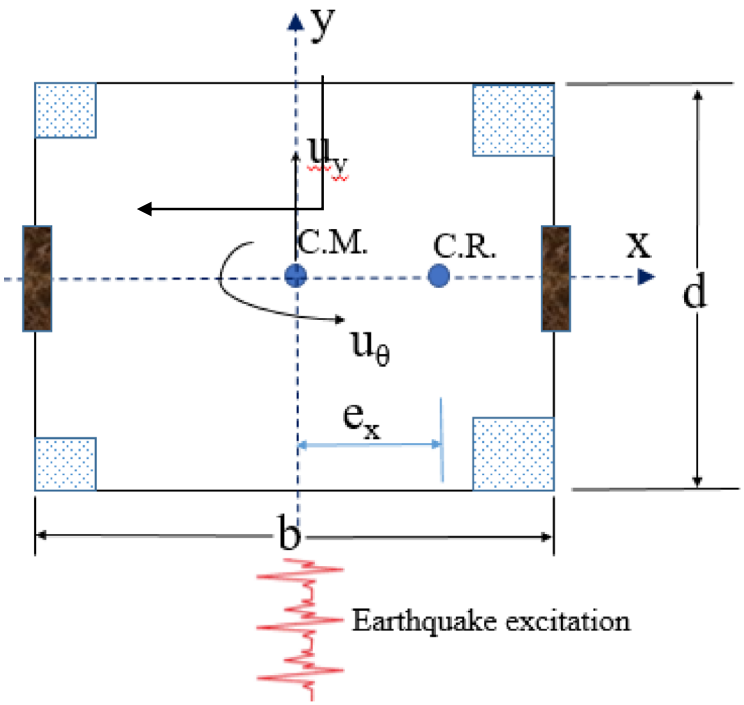

(a) Plan of the building

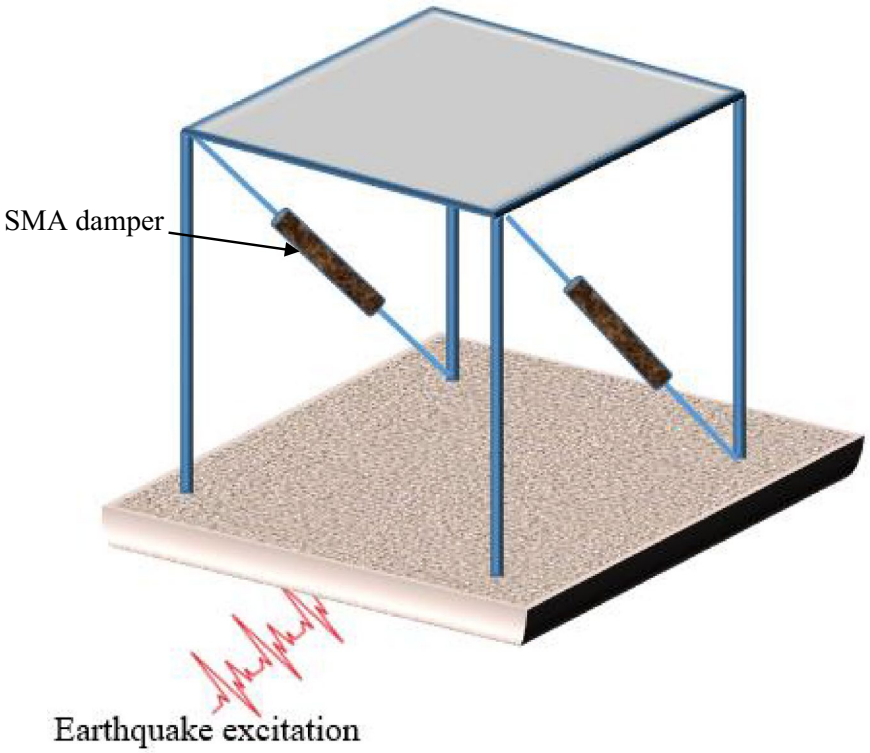

(b) Isometric view of the building

Fig. 4 Plan and isometric view of single-story plan asymmetric building (Parghi et al., 2024)

$$K = K_y \begin{bmatrix} 1 & e_x \\ e_x & \omega^2 l^2 \end{bmatrix} \tag{5}$$

where l is the mass-radius of gyration about a vertical axis through C.M., which is given by $l = \sqrt{\frac{b^2+d^2}{12}}$, where b and d are the plan dimensions of the building. ω represents the frequency ratio, given by $\omega = \frac{\omega_\theta}{\omega_y}$. ω_θ, and ω_y are torsional and lateral frequencies of the system, respectively as given in Eqs. (6–8).

$$\omega_\theta = \sqrt{\frac{K_{\theta l}}{ml^2}} \tag{6}$$

$$\omega_y = \sqrt{\frac{K_y}{m}} \tag{7}$$

$$K_{\theta l} = K_{\theta\theta} - e_x^2 K_y \text{ and } K_{\theta\theta} = \sum_i K_{xi} y_i^2 + \sum_i K_{yi} x_i^2 \tag{8}$$

In this context, K_y denotes the aggregate lateral stiffness of the structure in the y-direction. At the same time, e_x defines the eccentricity caused by the offset between the center of mass (CM) and the center of rigidity (CR). K_{yi}, represents the stiffness contribution of the *ith* column in the y-direction, and x_i indicates the horizontal coordinate of the *ith* column relative to the center of mass. The term $K_{\theta l}$ characterizes the rotational stiffness about a vertical axis through the center of rigidity (CR); simultaneously, $K_{\theta\theta}$ captures the rotational stiffness about a vertical axis through the center of mass (CM). Additionally, K_{xi} quantifies the lateral rigidity of the *ith* column in the x-direction, and y_i represents the vertical distance of the *ith* column from the center of mass.

Rayleigh damping is used to create the damping matrix of the system, which is not explicitly defined and expressed as $C_d = a_0 M + a_1 K$, where mass (M) and stiffness (K) are regarded. Where a_0 and a_1 are coefficients dependent on the damping ratios of two consecutive modes, this study considers a 5% damping ratio for both modes (Fig. 5).

Numerical study

The nonlinear time history analysis of the structure, as described in Sect. "Structural modeling", is performed using MATLAB (MathWorks, 2022). The study focuses on various

Table 1 Range of input parameters used for numerical study

Parameters	Minimum	Maximum	No. of values
Time period (T_y)	0.5	1.2	08
Frequency ratio (ω)	0.8	1.4	04
Eccentricity ratio (e_x/l)	0.0	1.0	11

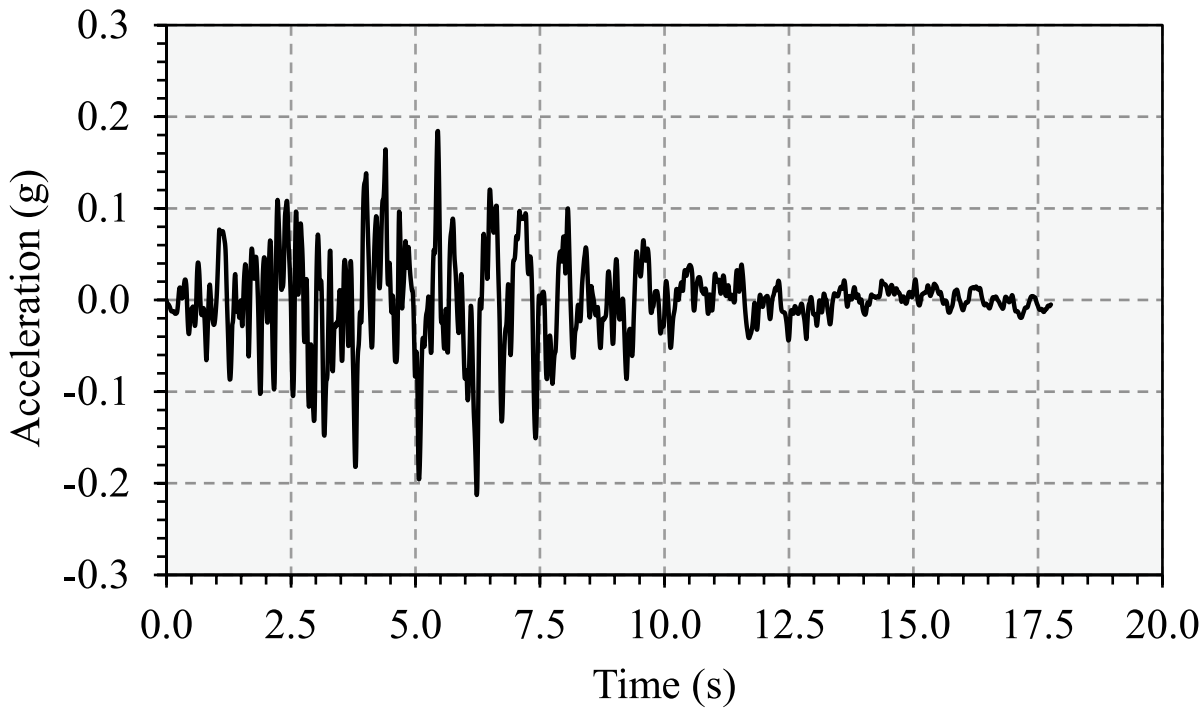

Fig. 5 Synthetic ground motions applied to the structure

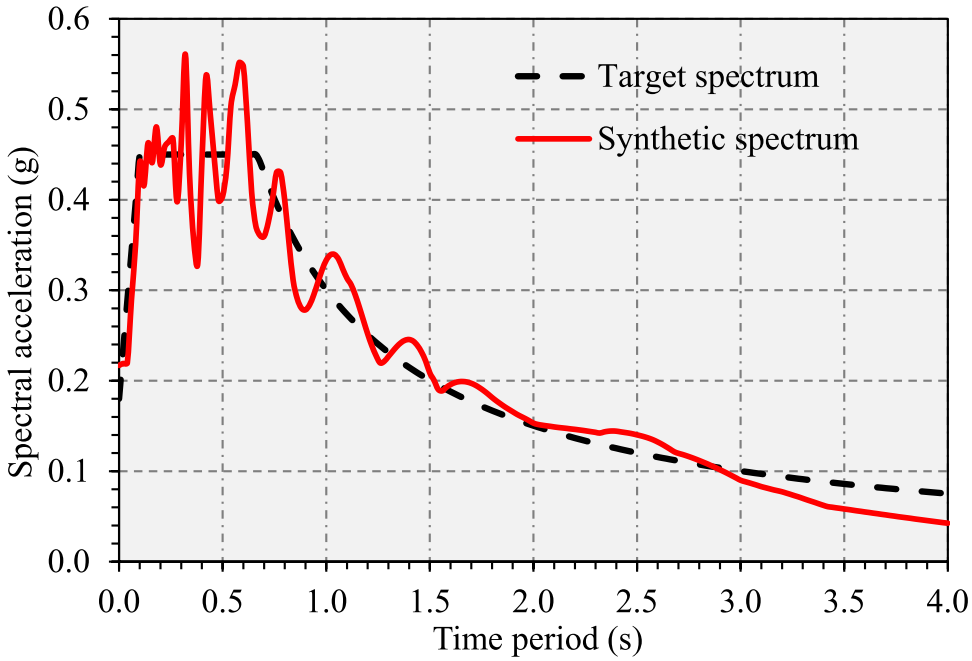

Fig. 6 Response spectra of selected ground motion

response parameters, such as lateral and torsional displacements at the floor's center of mass, displacements at the flexible and stiff edges, floor accelerations in both lateral and torsional directions, base shear, and forces restored by dampers at specific locations. Key parameters investigated include the eccentricity ratio (e_x/l), the uncoupled lateral period (T_y), and the ratio of uncoupled torsional to lateral frequencies ($\omega = \omega_\theta/\omega_y$). A summary of these parameters is presented in Table 1.

Figure 6 compares elastic response spectra derived from synthetic ground motions and target spectra. The analysis assumes a total building weight of 5000 kg. We Adjusted the column dimensions to achieve the uncoupled time period (T_y). The numerical study uses a floor plan with 3 m × 3 m dimensions. The performance of the implemented passive control system is assessed by quantifying its response through the response ratio (R_c), which is expressed as Eq. (9):

$$\mathrm{R_c} = \frac{\text{RMS response of structure controlled with SMA damper}}{\text{RMS response of uncontrolled structure}} \tag{9}$$

The $R_c < 1$ indicates an effective control system. In contrast, the root mean square (RMS) response of the controlled structure is less than that of the uncontrolled structure, showing that the control system successfully reduces the dynamic response. The $R_c = 1$ represents that the control system does not have an effect, as the RMS responses are equal for controlled and uncontrolled cases. There is no reduction in the structural response brought about by the control system. The $R_c > 1$ suggests that the control system is ineffective or even detrimental, as the RMS response of the controlled structure is greater than that of the uncontrolled structure. The $Rc > 1$ could mean that the control measures amplify the dynamic response rather than reduce it.

Framework for regression-based ML approach

In this study, we employed an ML approach to train a dataset comprising the responses of 352 time-period, eccentricity ratio, and frequency ratio combinations. We utilized the regression learner tool in MATLAB to facilitate this training process (MathWorks, 2022). The original responses for these combinations were generated through time history analysis of the structure, providing a robust dataset for model training. Once the team trained the network, they tested it with 10 combinations of predictors to evaluate its performance. The predicted responses from the trained network were then compared with the original responses using various ML methods to assess accuracy and effectiveness.

Artificial neural network

The structure and function of the human brain inspired the development of the ANN model, which recognizes patterns and tackles complex problems. It comprises layers of connected neurons, and learning methods like backpropagation improve the synoptic weight of each component (Goodfellow et al. 2016). ANNs excel in various applications,

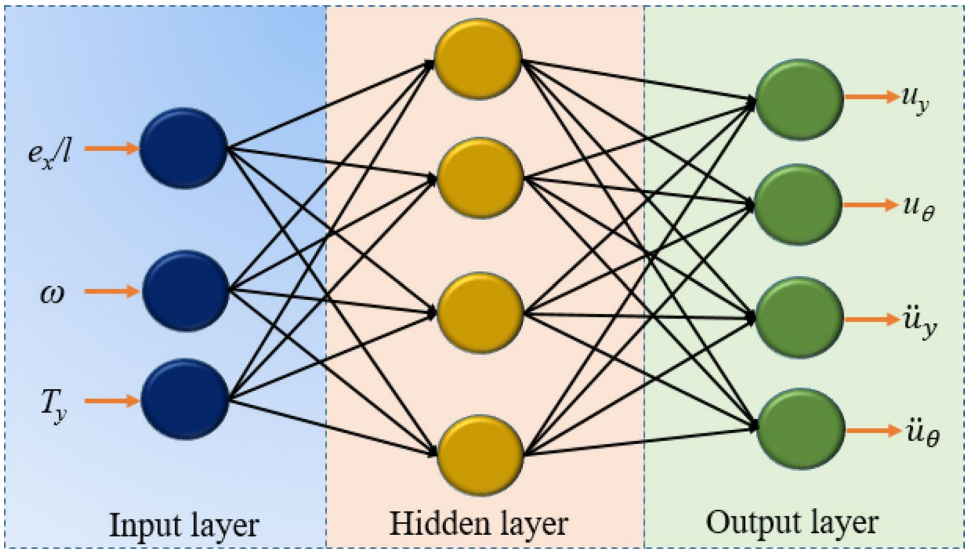

Fig. 7 Schematic diagram of ANN structure

including structural engineering, where engineers use them for tasks such as structural health monitoring (Altabey & Noori, 2022), detecting damage (Tran-Ngoc et al., 2022), and optimizing structural systems (Udaya Mohanan et al., 2023). With an SMA damper equipped, this study uses feed-forward networks to predict the structure's response. Figure 7 shows a schematic diagram of the ANN network.

The system's input and output layers correspond to its independent and dependent variables, respectively, with each data point represented by a single neuron in these layers. The hidden layer, which adjusts weights and performs data transformations, is referred to as "hidden" because its neuron count is not directly tied to the input or output data, and there is no universal rule to determine the precise number of neurons required. The operation of a hidden or output unit in the ANN is represented as Eq. (10) (Yucel et al., 2019):

$$y_j = f\left(\sum_i w_{ji} x_i + b_j\right) \tag{10}$$

In this expression, $i = 1,2,3,4$ and $j = 1,2,3$. Here, y_j represents the transformed output of the *jth* hidden or output neuron, $f(\cdot)$ is the activation function, w_{ij} denotes the synaptic weight between the *ith* input and the *jth* neuron, x_i is the input from the *ith* node, and b_j is the bias associated with the *jth* neuron.

Decision tree

Numerous industries generally use a decision tree (DT) to support decision-making. It employs a tree-structured modeling approach to explore possible outcomes of related choices (Yan et al., 2016). Data miners also use decision trees to classify and predict target variables. They construct classification or regression models using a tree-like structure, with classification trees applied to discrete target variables and regression trees to continuous target variables (Sishi & Telukdarie, 2021; Yan et al., 2016). We split a dataset into smaller subgroups, eventually developing into an associated tree with decision and leaf nodes. Decision nodes contain two or more branches, each representing a value of the tested attribute, while leaf nodes represent the final decision or outcome. The root node, considered the best predictor, sits at the top of the tree (Zhao et al., 2014). DTs can handle statistical and categorical data (Candanedo & Feldheim, 2016). One of the primary advantages of DTs over other modeling techniques is their ability to visually represent data through branch diagrams that convey effective If–Then rules (Yan et al., 2016). Each leaf in a DT represents a decision rule that includes metadata, and DTs highlight the value and influence of independent variables (Candanedo & Feldheim, 2016).

Support vector machine

Unlike traditional SVM, which focuses on maximizing margins to classify data into distinct categories, support vector regression (SVR) aims to derive a function that closely approximates all data points within a defined tolerance range (Wei et al., 2024). Unlike SVM, SVR utilizes a loss function independent of the ε parameter to construct the hyperplane.

This hyperplane is designed to ensure that the predicted response values for the training data stay within the ε-insensitive region, which is the range of values that can be accepted around the actual observed values, as shown in Fig. 8. The SVR model strives to position as many data points as possible within this ε-insensitive region. Points

falling inside this region do not contribute to the model's loss function, while points outside the region significantly influence the loss. This feature allows SVR to maintain robustness by being unaffected by variations within the ε-insensitive range. The standard method for identifying this function involves minimizing the following objective function as Eqs. (11) and (12) (Feng et al., 2020):

$$\text{minimize}\frac{1}{2}\|w\|^2 + c\sum_{i=1}^{n}\left(\xi_i + \xi_i^*\right) \tag{11}$$

$$\textit{subject to}\begin{cases} q_i - \langle w, p_i\rangle - m \le \varepsilon + \xi_i \\ \langle w, p_i\rangle + m - q_i \le \varepsilon + \xi_i \\ \xi_i, \xi_i^* \ge 0, i = 1, 2, ..., n \end{cases} \tag{12}$$

here w represents the weight vector that defines the decision boundary, and c is the penalty parameter used to manage the error term and mitigate overfitting. The slack variables ξ_i^* permit specific data points to lie outside the ε -tube. Additionally, p_i refers to the feature vector for the *ith* training sample, y_i denotes the target value for the same sample, n is the total number of training samples, and m represents the bias term.

Ensemble bagged tree

The ensemble bagged tree (EBT) algorithm is a powerful ML technique that combines multiple decision trees to enhance the stability and accuracy of predictions. "Bagged" refers to bootstrap aggregation, in which random sampling generates different subsets of data, and multiple decision trees train on these subsets. By aggregating predictions from these individual trees, the EBT reduces the variance often affecting single decision trees, thereby improving the model's overall performance (Breiman, 1996).

Each tree in an ensemble is grown independently, ensuring diversity, which is crucial for reducing overfitting. During prediction, the algorithm uses either a majority vote (for classification tasks) or an average (for regression tasks) from all the trees, resulting in a robust prediction that benefits from the diverse perspectives of each tree. This approach makes the EBT particularly effective in handling noisy datasets and complex relationships. In scenarios where accuracy is paramount, and the training dataset is prone to high variance or contains noise, users often employ the EBT algorithm. By leveraging the advantages of both decision trees and ensemble learning, it achieves a high level of generalizability while maintaining the interpretability of the decision tree model (Yang et al., 2024).

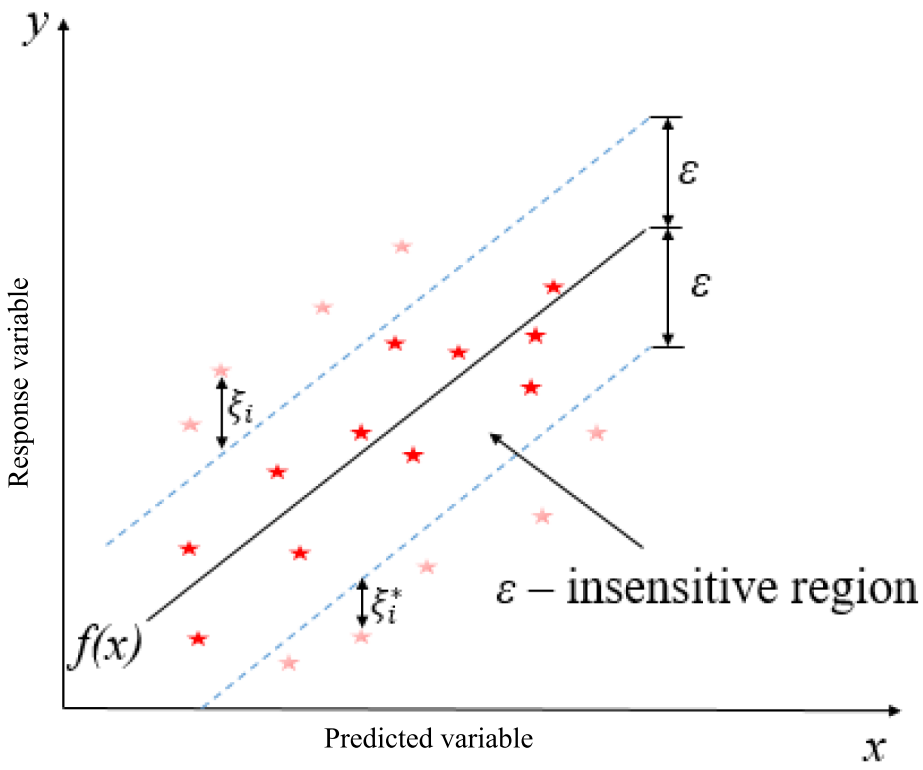

Fig. 8 Schematic representation of SVM structure

Gaussian process regression

Gaussian process regression (GPR) is a non-parametric, probabilistic approach used in ML for regression tasks. It is beneficial in scenarios where the correlation between input and output variables is complex and precise predictions are needed. The concept of a Gaussian process forms the basis of GPR, as it represents a distribution over probable functions that fit the data. In GPR, the idea is to place a prior distribution over the function space representing the relationship between inputs and outputs rather than directly modeling parameters. As a result, instead of offering a single best estimate, GPR might offer a distribution over possible functions consistent with the data. The core components of a GPR model are the mean function and covariance (or kernel) function. The mean function represents the predictable value, while the kernel function defines the covariance between any two points in the input space, thus controlling the smoothness and complexity of the predicted function (Zhong et al., 2023). Mathematically, GPR assumes that the observed data points follow a multivariate normal distribution, with the joint distribution of the training data and the new test points described by Eq. (13):

$$f(x) \sim \mathbb{N}(\mu(x), k(x, x')) \tag{13}$$

where μ(x) represents the mean function, which defines the predictable value of the function at any given point x. For simplicity, the mean function is often set to zero, especially when there is no prior knowledge about the function's expected behavior. This allows the model to focus purely on variations captured by the covariance structure. The kernel function k (x, x'), on the other hand, plays a critical role in GPR as it defines the similarity between two data points x and x'. This function determines the covariance between function values at these points, thereby controlling the smoothness, amplitude, and overall structure of the function being modeled. The GPR model is highly valued for its ability to quantify uncertainty in its predictions, a significant advantage in engineering applications. It can provide not only the predicted mean but also the variance, which gives insights into the confidence of the predictions.

Hyperparameter optimization

Hyperparameter optimization is a vital process in machine learning that focuses on adjusting hyperparameters to enhance a model's performance. Unlike model parameters, which are learned from data during training, hyperparameters are predefined before the training begins and dictate how the model learns. Hyperparameters control the training algorithm's behavior and significantly affect a machine learning model's performance and generalization ability. Better accuracy, faster convergence, and enhanced generalization to unknown data (Li et al., 2021) can all follow from optimal hyperparameter choices. This paper uses the grid search method for hyperparameter optimization. Table 2 displays the parameters optimized for each machine-learning model.

Performance index for machine learning algorithms

The performance metric of the ML model primarily measures the error between the predicted and target values of structural responses. The ML models applied to regression tasks, metrics such as the coefficient of determination (R^2) Eq. (14), mean squared error (MSE) Eq. (15), root mean squared error (RMSE) Eq. (16), and mean absolute error (MAE) Eq. (17) are used to evaluate the performance of each regression model in this study.

$$R^2(x, \widehat{x}) = 1 - \frac{\sum_{i=1}^{n} (x_i - \widehat{x}_i)^2}{\sum_{i=1}^{n} (x_i - x)^2} \tag{14}$$

$$MSE(x, \widehat{x}) = \frac{1}{n} \sum_{i=1}^{n} (x_i - \widehat{x}_i)^2 \tag{15}$$

$$RMSE(x, \widehat{x}) = \sqrt{\left(\frac{1}{n} \sum_{i=1}^{n} (x_i - \widehat{x}_i)^2 \right)} \tag{16}$$

$$MAE(x, \widehat{x}) = \frac{1}{n} \sum_{i=1}^{n} \left| x_i - \widehat{x}_i \right| \tag{17}$$

Result and discussion

This section presents the findings of the numerical simulations using a nonlinear time history analysis of the structure subjected to synthetic ground motion. The analysis generated numerical results for 352 combinations of structural parameters, including time period, eccentricity ratio, and frequency ratio. These results were subsequently utilized as input data for ML models. This study evaluated five ML algorithms: ANN, DT, EBT, SVM, and GPR. The primary objective was to assess the effectiveness of these regression algorithms in predicting the seismic response of asymmetric structures equipped with SMA dampers.

Table 2 Hyper parameters for different models in machine learning

Model	Hyper parameters	Value
ANN	Hidden layer size	10
	solver	Lbfsg
	Activation	Sigmoid
DT	Minimum leaf size	12
	Minimum samples split	2
SVM	Kernal function	Gaussian
	Kernal scale	0.43
EBT	Minimul leaf size	8
	Number of learners	30
GPR	Kernal function	Squared exponential
	Optimizer	quasinewton

Response of the structure under synthetic ground motion

The numerical simulations were performed on a structure featuring two distinct dampers on opposite sides to investigate their effectiveness in mitigating seismic responses. Figure 9 illustrates the response histories of the structure under synthetic ground motions, both with and without the inclusion of SMA dampers. The structural responses, including lateral displacement (u_y), torsional displacement (u_θ), lateral acceleration ($\ddot{u}_y$), torsional acceleration ($\ddot{u}_\theta$), flexible edge displacement (u_{yf}), and stiff edge displacement (u_{ys}), are plotted against time to provide a comprehensive analysis of the system's behavior. In the plots, the red solid line represents the responses of the structure equipped with SMA dampers, while the black dotted line corresponds to the uncontrolled structure without dampers. A clear distinction between the two response scenarios can be observed in all plots. Including SMA dampers significantly reduces the structural responses, including displacements and accelerations, when subjected to earthquake ground motion. This demonstrates the effectiveness of SMA dampers in mitigating seismic effects and enhancing structural performance under dynamic loading conditions.

Table 3 shows the structure's peak and root mean square (RMS) response for selected T_y, ω, and e_x/l combinations. The third column under each response category highlights the percentage reduction in the response of the controlled structure compared to the uncontrolled structure. The results indicate that SMA dampers effectively mitigate both peak and RMS values of lateral displacement (u_y), torsional displacement (u_θ), lateral acceleration ($\ddot{u}_y$), and torsional acceleration ($\ddot{u}_\theta$). The maximum reduction in peak response (10.45%) is observed in angular displacement for the structural parameter combination $T_y = 0.9$, $\omega = 0.8$, and $e_x/l = 0.5$. Similarly, the maximum decrease in RMS response (15.29%) is noted in lateral displacement for the parameter combination $T_y = 1.2$, $\omega = 1.2$, and $e_x/l = 1$.

Training model performance

Figure 10 presents the MAPE of five models—ANN, DT, SVM, EBT, and GPR—across six response variables (u_y, u_θ, $\ddot{u}_y$, $\ddot{u}_\theta$, f_{ds}, f_{df}). The models showed good predictive performance for most response variables (u_y, u_θ, $\ddot{u}_y$, $\ddot{u}_\theta$, f_{df}). The MAPE values were generally under 1.0 for all models except EBT, indicating high accuracy in the predicted structural responses compared to the actual values. The GPR model exhibited the lowest MAPE (0.04% in $\ddot{u}_y$) across all response variables, demonstrating superior accuracy overall. ANN, DT, and SVM also showed strong predictive performance for most response variables. Their MAPE values were mainly below 0.5, suggesting reliable accuracy. However, the EBT model showed notably higher MAPE values, especially for f_{ds} (9.69%), indicating a relatively lower predictive performance for these variables. Compared to u_y, u_θ, $\ddot{u}_y$, $\ddot{u}_\theta$, the response variables f_{ds} and f_{df} have relatively higher MAPE values across all prediction models, likely due to discrepancies in their input values.

Figure 11 compares the predicted and actual results for various prediction models in estimating angular displacement responses (u_θ). Among all models, GPR exhibits the closest alignment with the perfect prediction line, demonstrating its superior accuracy and ability to model uncertainties effectively. SVM also performs well, providing consistent and accurate predictions across the response range. While ANN captures non-linear relationships effectively, it shows some deviations at extreme response values. EBT and DT demonstrate moderate performance, with noticeable scatter indicating potential overfitting or limitations in capturing complex patterns. Overall, GPR stands out as the most reliable model, followed closely by SVM for practical applications.

Table 4 presents the performance of different ML algorithms (ANN, DT, SVM, EBT, GPR) on four response variables (u_y, u_θ, $\ddot{u}_y$, $\ddot{u}_\theta$). The performance metrics used for evaluation are RMSE, R^2, prediction speed (obs/sec), and training time (sec). Generally, GPR consistently exhibits the lowest RMSE and highest R^2 across all response variables, indicating the most accurate predictions among the algorithms. For instance, GPR achieves an R^2 value of 0.99 for both 'u_θ' and '$\ddot{u}_\theta$, with correspondingly low RMSE values (0.0032 and 0.0031, respectively). This suggests GPR's superior ability to capture the underlying relationships in the data. DT also performs well with competitive accuracy and efficient training times, providing a good balance between accuracy and computational efficiency. SVM excels in prediction speed and training efficiency, making it ideal for real-time applications, although it lacks the accuracy

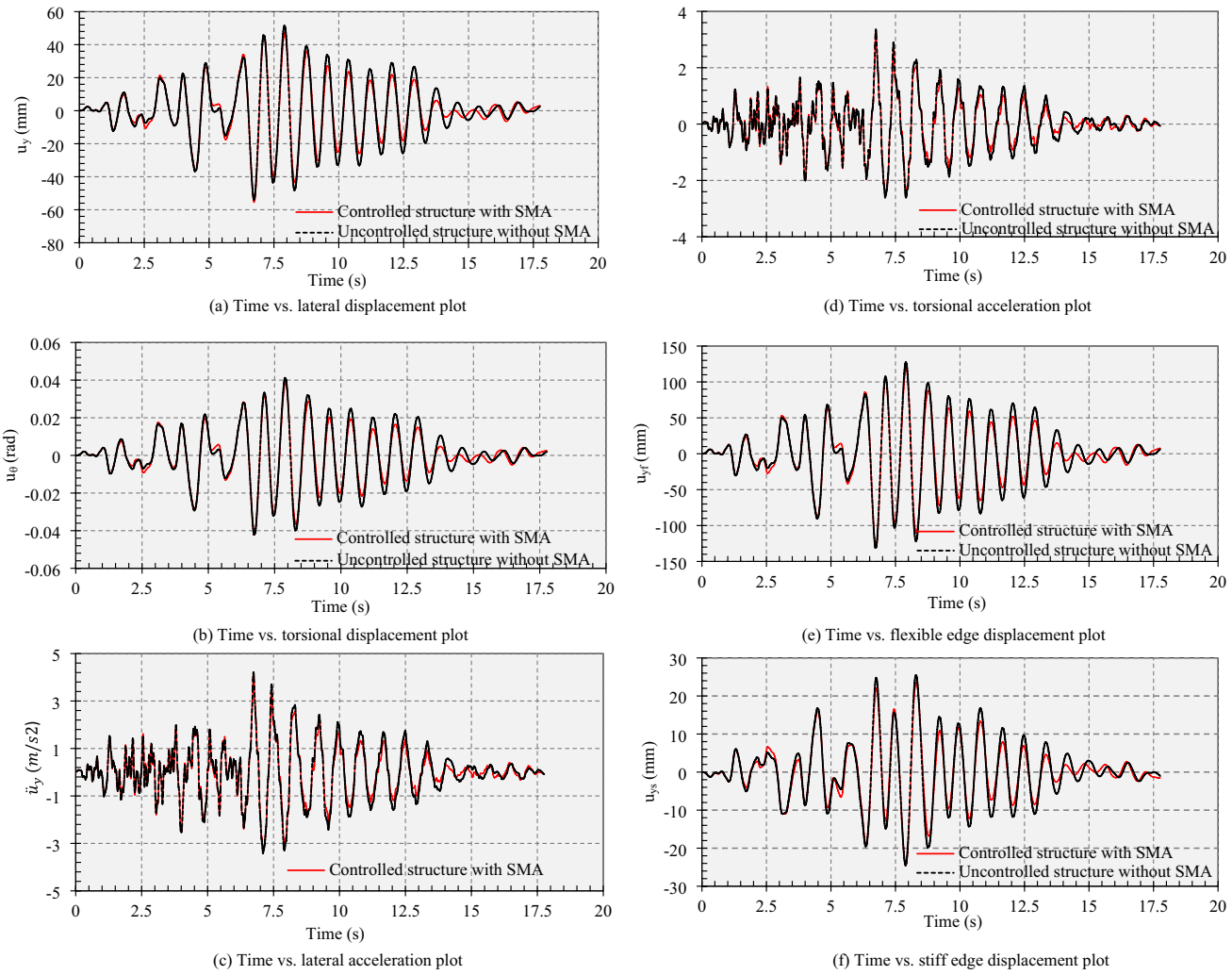

Fig. 9 Time histories of structural response controlled with SMA damper and without damper under synthetic ground motion ($T_y = 1$, $e_x/l = 0.3$, $\omega = 1$)

of GPR and DT. ANN offers consistent performance but does not outperform GPR or DT in any specific metric. EBT has the lowest accuracy and prediction speed, making it the least favourable choice. The choice of algorithm ultimately depends on whether accuracy, speed, or a balance of both are the most critical factors for the application.

Figure 12 illustrates the predicted versus actual values for f_{df} across all ML models, highlighting the variations in performance among the algorithms. The ANN plot reveals a close alignment between the actual and predicted responses, with a minimal and relatively uniform error magnitude throughout the dataset. The DT model captures some of the general trends in the data; there are noticeable discrepancies between the predicted and actual values. Errors are inconsistent and vary significantly across the records, with some points showing relatively large deviations. For SVM, the errors between actual and predicted results are noticeably larger, indicating that the SVM struggles with some outliers in the data. The error lines in the EBT model are relatively long, indicating significant deviation for specific records, particularly at extreme values. The GPR plot shows high alignment between the predicted and actual values, with relatively small and evenly distributed error magnitudes. The GPR model demonstrates the best performance with minimal errors between actual and predicted values.

Figure 13 illustrates the performance of various ML models (ANN, SVM, GPR, fine tree, and EBT) compared to actual results across a range of frequency ratios (ω). The *y*-axis represents the response ratio for u_y, u_θ, $\ddot{u}_y$, $\ddot{u}_\theta$ which are structural response parameters of nonlinear time history analysis. All models generally follow the trend of the actual results, but their deviations indicate varying degrees of accuracy. The DT and GPR closely follow the line of actual results, shown by the black line in Fig. 13. ANN also

Table 3 Peak and RMS response of the structure with selected cases under synthetic ground motion

Combinations				u_y (m)			u_θ			$\ddot{u}_y$			$\ddot{u}_\theta$		
T_y	ω	e_x/l		U	C	R (%)	U	C	R (%)	U	C	R (%)	U	C	R (%)
0.6	1.2	1	Peak	0.054	0.049	09.324	0.059	0.057	3.085	3.676	3.454	6.052	6.222	5.945	04.443
			RMS	0.013	0.012	11.724	0.013	0.012	6.314	0.954	0.901	5.546	1.415	1.333	05.782
0.7	0.8	0.5	Peak	0.078	0.071	09.579	0.057	0.051	10.718	5.095	4.885	4.129	4.123	3.850	06.620
			RMS	0.025	0.022	11.661	0.019	0.016	12.189	1.478	1.315	11.081	1.145	1.024	10.552
0.7	1.2	1	Peak	0.056	0.050	09.695	0.059	0.057	2.849	3.698	3.470	6.171	6.223	5.951	04.374
			RMS	0.014	0.012	12.630	0.013	0.012	6.511	0.956	0.902	5.648	1.414	1.332	05.768
0.8	0.8	0.5	Peak	0.079	0.071	09.761	0.057	0.051	10.770	5.105	4.894	4.130	4.133	3.858	06.653
			RMS	0.025	0.022	11.726	0.019	0.016	12.344	1.478	1.315	11.074	1.145	1.024	10.562
0.8	1.2	1	Peak	0.057	0.051	09.939	0.059	0.057	2.601	3.684	3.453	6.269	6.166	5.900	04.306
			RMS	0.014	0.012	13.377	0.013	0.012	6.669	0.951	0.897	5.710	1.400	1.320	05.708
0.9	0.8	0.5	Peak	0.079	0.071	09.645	0.058	0.051	10.845	5.100	4.892	4.077	4.132	3.856	06.679
			RMS	0.025	0.022	11.714	0.018	0.016	12.403	1.467	1.306	10.983	1.136	1.017	10.478
0.9	1.2	1	Peak	0.057	0.051	10.139	0.058	0.057	2.409	3.646	3.414	6.351	6.072	5.812	04.277
			RMS	0.015	0.013	14.018	0.013	0.012	6.838	0.941	0.887	5.755	1.379	1.301	05.643
1	1	0.9	Peak	0.043	0.039	09.299	0.049	0.047	4.968	3.553	3.426	3.561	4.075	3.918	03.860
			RMS	0.011	0.010	11.104	0.012	0.012	7.412	0.998	0.931	6.648	1.206	1.124	06.802
1	1.2	1	Peak	0.057	0.051	10.240	0.057	0.056	2.220	3.592	3.360	6.453	5.955	5.702	04.246
			RMS	0.015	0.013	14.528	0.013	0.012	6.977	0.929	0.875	5.780	1.353	1.278	05.561
1.1	1	0.9	Peak	0.043	0.039	09.465	0.049	0.047	5.166	3.520	3.397	3.481	4.057	3.893	04.037
			RMS	0.011	0.010	11.316	0.012	0.011	7.302	0.981	0.918	6.421	1.185	1.107	06.561
1.1	1.2	1	Peak	0.057	0.051	10.348	0.056	0.055	2.042	3.527	3.295	6.577	5.823	5.578	04.209
			RMS	0.015	0.013	14.956	0.013	0.012	7.093	0.915	0.862	5.792	1.325	1.252	05.464
1.2	1	0.9	Peak	0.043	0.039	09.543	0.049	0.046	5.298	3.482	3.365	3.364	4.032	3.863	04.194
			RMS	0.011	0.010	11.447	0.012	0.011	7.159	0.964	0.905	6.174	1.163	1.089	06.301
1.2	1.2	1	Peak	0.057	0.051	10.453	0.055	0.054	1.914	3.456	3.224	6.724	5.684	5.444	04.207
			RMS	0.015	0.013	15.299	0.013	0.012	7.211	0.900	0.847	5.799	1.296	1.226	05.378

U = uncontrolled structure, C = controlled structure with SMA damper, R = reduction in response

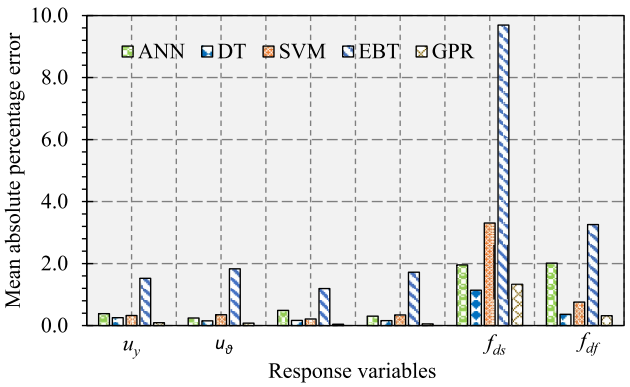

Fig. 10 MAPE values for different ML approaches across response variables

gives good results but is less accurate than DT and GPR. The SVM slightly deviates from accurate results as it shows a minor error in prediction. The analysis reveals that the EBT does not serve as a precise model, as it demonstrates varying trends compared to the actual results. Table 5 provides a detailed comparison of the MAPE for five ML algorithms ANN, DT, SVM, EBT, and GPR across various structural responses ratio u_y, u_θ, $\ddot{u}_y$, $\ddot{u}_\theta$. We compute the errors for selected test cases using different combination of T_y, ω and e_x/l.

The results revealed that the GPR is the most accurate and reliable model for predicting structural responses. Its consistently low MAPE (1.42% in u_y, 0.73% in u_θ, 1.03% in $\ddot{u}_y$, 0.83% in $\ddot{u}_\theta$) values across all response variables indicate robust performance and high prediction accuracy. DT also performs well, particularly in predicting u_θ with minimal errors, making it a strong candidate for applications requiring reliable predictions with lower computational costs. SVM shows the highest variability (2.46% in u_y) and generally poor performance across all response variables. This implies that SVM might not be appropriate for this dataset and issue, particularly considering its reduced accuracy and increased computational requirements. EBT displays a wide range of errors (3.42% in u_y), indicating inconsistent

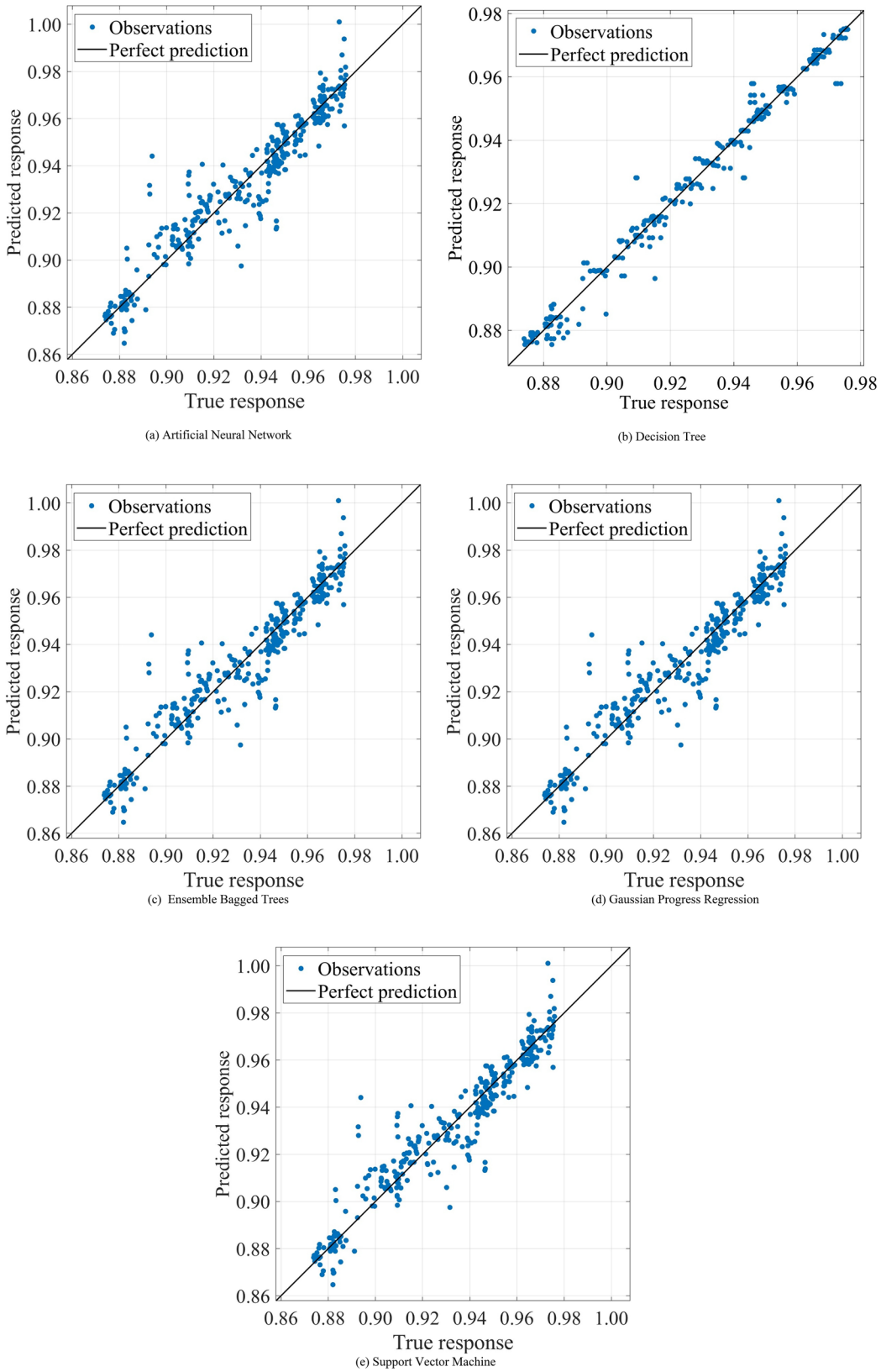

Fig. 11 Predicted versus actual results for different models for u_θ response

Table 4 Training parameters for different machine learning algorithms

Response	Algorithm	RMSE	R^2	Prediction speed (obs/s)	Training time (s)
u_y	ANN	0.0066	0.9500	3200	37.13
	DT	0.0072	0.9400	2900	**34.14**
	SVM	0.0111	0.8500	7100	46.23
	EBT	0.0201	0.6000	1200	38.32
	GPR	**0.0050**	**0.9700**	**3500**	48.42
u_θ	ANN	0.0093	0.9000	500	50.18
	DT	0.0043	0.9800	830	20.75
	SVM	0.0107	0.8700	1100	**07.93**
	EBT	0.0230	0.6100	430	38.10
	GPR	**0.0032**	**0.9900**	**3800**	53.35
$\ddot{u}_y$	ANN	0.0084	0.8200	2600	30.63
	DT	0.0047	0.9400	**5700**	**07.68**
	SVM	0.0083	0.8300	9100	02.47
	EBT	0.0157	0.6800	0560	23.48
	GPR	**0.0030**	**0.9800**	2100	35.08
$\ddot{u}_\theta$	ANN	0.0076	0.9100	**3100**	56.78
	DT	0.0047	0.9700	860	28.20
	SVM	0.0101	0.8400	5500	**02.89**
	EBT	0.0203	0.7100	790	38.40
	GPR	**0.0031**	**0.9800**	3000	48.18

The bold numbers show the best value for that particular parameter, expressing the best algorithm for the training ofthat particular parameter

For RMSE and training time, the lowest value is best

For R^2, the highest value is best

performance. While it performs adequately in some cases (1.89% in $\ddot{u}_y$), its higher error rates in others make it less reliable than GPR and DT.

Feature impact analysis using SHapley additive exPlanations (SHAP)

Introduction of SHAP

While the GPR and DT models provide accurate and rapid predictions of the structure's responses under seismic loading, comprehending the underlying mechanisms remains challenging. To find a solution to this problem, we have created several different interpretations and approaches for machine learning models. In this study, we utilized SHAP (Sun et al., 2022) to analyze the impact of various inputs on SMA damper performance. SHAP is a versatile interpretation method applicable to any ML model. Rooted in game theory, it utilizes an additive feature attribution framework. Each feature's contribution is quantified using the Shapley value, representing the model's output as a linear combination of these feature contributions. The SHAP model, $S(x)$, can be expressed as Eq. (18):

$$S(x) = \phi_0 + \sum_{i=1}^{n} \phi_i x_i \tag{18}$$

In this formulation, x signifies a transformed input derived from the original input, defined as.

$x = h_x(x)$. The term ϕ_0 represents the mean prediction of the machine learning model, which serves as the default output when no input features are provided. The contribution of each feature is captured by ϕ_i, also referred to as the Shapley value for that specific feature, while n indicates the total count of features considered. Unlike traditional methods prioritizing ranking feature importance, SHAP offers a dual perspective by combining global and local interpretations of the model. It provides a deeper understanding of how each feature contributes to the model's overall output and reveals the specific impact of individual features on predictions.

Feature impact analysis

This study uses SHAP to assess the impact of various input variables on the model's output. The SHAP analysis is based on the trained DT model developed using the response data. Figure 14 provides a detailed visualization of how each input variable influences the response ratio for torsional displacement.

Figure 14a depicts the SHAP summary plot, which illustrates the distribution of SHAP values for each feature (e.g., e_x/l, ω, T_y) across all data instances. The x-axis represents the SHAP value, indicating the feature's effect on the model's output, while the y-axis lists the features in descending order of importance. Each point is color-coded, ranging from blue (low feature values) to red (high feature values), offering insights into whether high or low values of a feature contribute positively or negatively to the response ratio.

Figure 14a shows that e_x/l and ω have substantially influenced the model's output, with a mix of positive and negative SHAP values. The mix of positive and negative SHAP values suggests a complex, context-dependent relationship with the response ratio. For instance, high values of e_x/l tend to increase the response ratio, while lower values tend to reduce it. In contrast, T_y shows a smaller and more centralized distribution of SHAP values, indicating a limited effect on the output. Figure 14b presents each feature's mean absolute SHAP values, summarizing their overall impact on the model. We can see that e_x/l and ω are the most significant factors affecting the response ratio for torsional displacement, while T_y has a minimal influence. This phenomenon highlights the importance of accurately

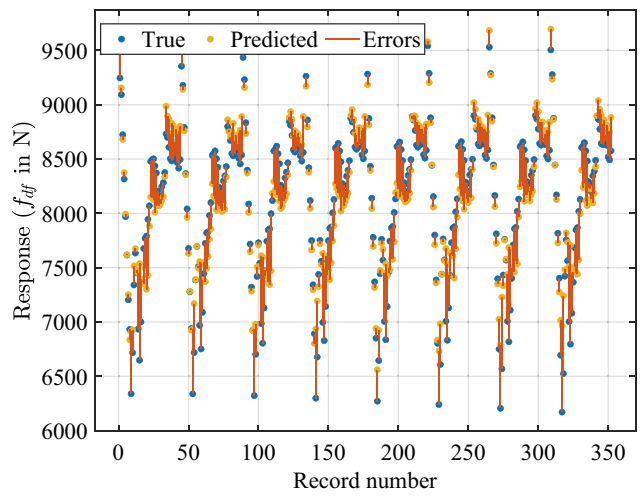

(a) Artificial Neural Network

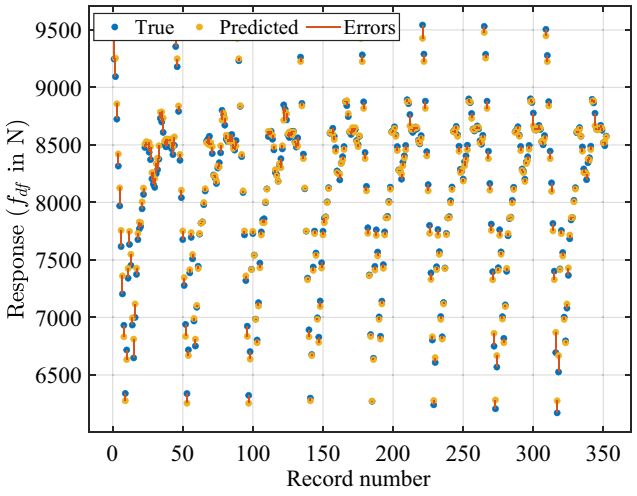

(b) Decision Tree

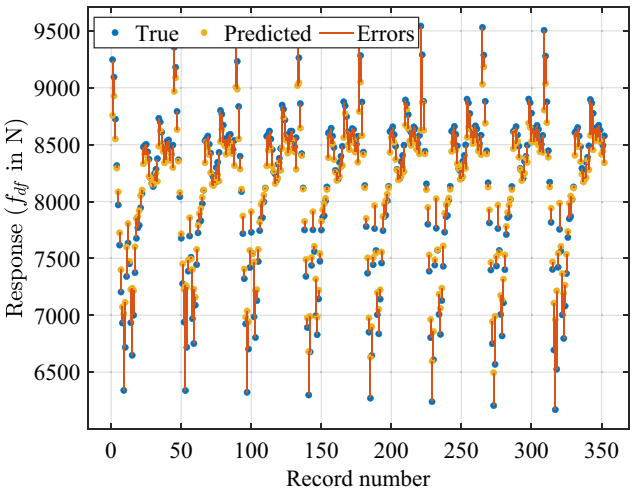

(c) Support Vector Machine

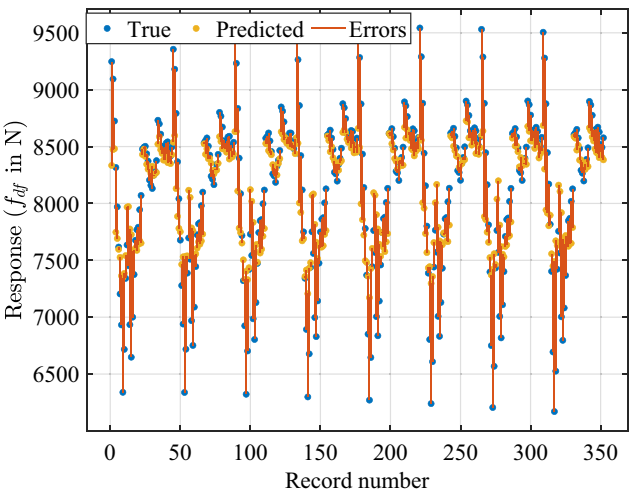

(d) Ensemble Bagged Trees

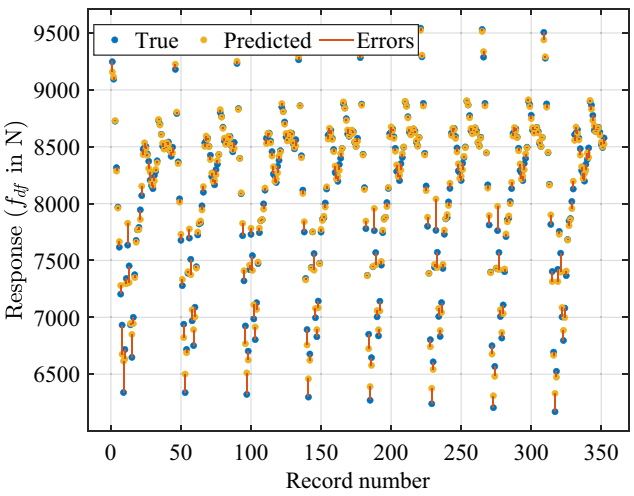

(e) Gaussian Process Regression

Fig. 12 Response plot of different algorithm predictions for flexible edge displacement force (f_{df})

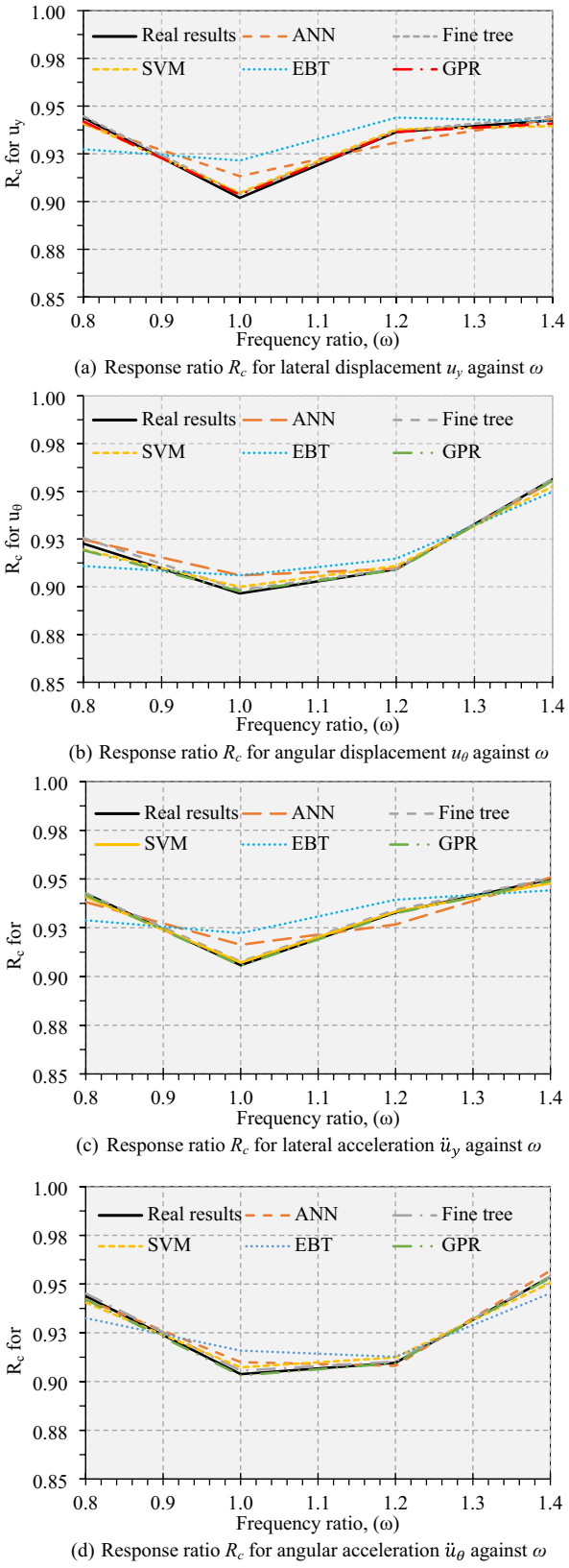

(a) Response ratio R_c for lateral displacement u_y against ω

(b) Response ratio R_c for angular displacement u_θ against ω

(c) Response ratio R_c for lateral acceleration $\ddot{u}_y$ against ω

(d) Response ratio R_c for angular acceleration $\ddot{u}_\theta$ against ω

Fig. 13 Variation in response ratio (R_c) with varying frequency ratio (ω) and different Machine Learning algorithms

measuring and considering e_x/l and ω in model predictions, as they have the highest impact on the output.

To better demonstrate how the features influence the output of the ML model, Fig. 13 presents feature dependence plots for ω, T_y, and e_x/l. In these plots, the x-axis represents the range of the input variable, while the y-axis displays the corresponding SHAP value, reflecting the feature's contribution to the model output. The shading in the plots indicates the impact of a secondary input variable on the SHAP values.

Figure 15a shows that when ω is below a certain threshold, its impact on the output is minimal. However, as ω increases, the SHAP value for ω also increases, suggesting a more substantial influence on the model's predictions. The color shading represents the influence of e_x/l, with higher values of e_x/l corresponding to greater SHAP values for ω. Similarly, in Fig. 15b, the SHAP values for T_y are shown to be relatively low for lower values of T_y, with a noticeable increase as T_y exceeds a specific range. The color shading again represents the impact of *ex*/*l* on the SHAP values for T_y, demonstrating that changes in e_x/l modify T_y's effect.

In Fig. 15c, the feature dependence plot for *ex*/*l* shows that the value of ω, represented by color shading, influences the SHAP values. This plot indicates that as *ex*/*l* increases, the corresponding SHAP values fluctuate, with a more substantial impact observed when ω is within a specific range. These results provide valuable insights into how the primary features interact with secondary variables, offering a clearer understanding of critical parameters in the model's predictive behavior.

Conclusions

Structural characteristics such as time period, frequency ratio, and eccentricity ratio are critical in defining how a structure responds to seismic occurrences. SMA wire dampers have proven effective at minimizing the response to torsionally linked structures. This research proposes several regression-based ML methods to predict the behavior of buildings with SMA wire dampers using modifications in the time period, frequency ratio, and eccentricity ratio. We also employed the SHAP method to investigate the factors significantly influencing the structural response. We have drawn the following conclusions based on the dynamic time history analysis, ML techniques, and regression model predictions.

1. The SMA wire damper effectively reduces the structural RMS response by up to 15% under synthetic ground motions, showcasing its ability to limit sustained oscillatory displacements and accelerations. This reduction enhances structural durability, minimizes cumulative

Table 5 Comparison of all model for MAPE in test case

T_y	ω	e_x/l	ANN (% error)				DT (% error)				SVM (% error)				EBT (% error)				GPR (% error)			
			u_y	u_θ	$\ddot{u}_y$	$\ddot{u}_\theta$	u_y	u_θ	$\ddot{u}_y$	$\ddot{u}_\theta$	u_y	u_θ	$\ddot{u}_y$	$\ddot{u}_\theta$	u_y	u_θ	$\ddot{u}_y$	$\ddot{u}_\theta$	u_y	u_θ	$\ddot{u}_y$	$\ddot{u}_\theta$
0.45	0.80	0.50	1.25	0.93	1.13	0.56	1.25	1.27	0.53	0.64	1.56	1.57	1.55	1.16	4.55	3.07	2.76	2.98	0.24	0.15	0.29	0.05
0.80	1.00	0.25	2.16	0.45	0.67	0.19	2.16	1.59	1.34	1.34	0.59	0.74	0.48	0.61	0.25	0.44	0.04	0.15	0.65	0.57	0.33	0.27
0.75	0.90	0.10	4.54	0.77	2.60	0.23	4.54	1.83	4.31	0.73	4.47	1.63	2.95	1.04	4.18	3.79	2.48	2.98	4.64	1.00	3.17	1.15
1.00	0.75	0.85	1.25	0.60	0.53	0.80	1.25	0.03	0.01	0.02	0.99	1.15	0.85	1.19	3.65	2.01	2.00	2.16	0.28	0.19	0.30	0.46
1.20	1.50	0.70	1.63	**7.92**	1.20	1.95	1.63	3.33	2.92	3.66	1.72	2.07	2.08	2.09	0.82	0.98	1.59	1.32	0.93	3.03	2.45	3.21
1.15	0.75	0.90	1.97	1.79	0.96	2.55	1.97	0.47	0.51	0.54	1.44	1.30	0.91	1.14	4.37	2.73	1.83	2.19	0.14	0.36	0.43	0.51
0.50	1.00	0.45	0.48	0.87	0.55	0.51	0.48	1.57	1.30	1.30	0.21	0.28	0.44	0.28	3.56	2.23	2.20	3.14	0.12	0.10	0.06	0.03
0.30	1.40	0.30	1.47	0.43	0.56	0.23	1.47	0.34	1.61	0.64	4.75	2.86	3.64	2.79	2.72	1.28	2.66	1.69	3.92	1.79	2.99	2.01
0.90	0.80	0.50	0.31	0.21	0.76	0.31	0.31	0.29	0.17	0.20	0.30	0.40	0.21	0.39	3.72	3.74	3.13	3.08	0.22	0.12	0.11	0.07
1.30	1.20	1.00	1.06	0.87	0.41	0.55	1.06	0.63	0.11	0.36	**8.60**	0.36	0.29	1.16	**6.64**	0.66	0.21	1.28	3.08	0.01	0.17	0.52
MAPE			1.61	1.49	0.94	0.79	1.61	1.13	1.28	0.94	2.46	1.24	1.34	1.19	3.45	2.09	1.89	2.10	1.42	0.73	1.03	0.83

ANN, artificial neural network; DT, decision trees; SVM, support vector machine; EBT, ensemble bagged trees; GPR, Gaussian process regression; MAPE, mean absolute percentage error

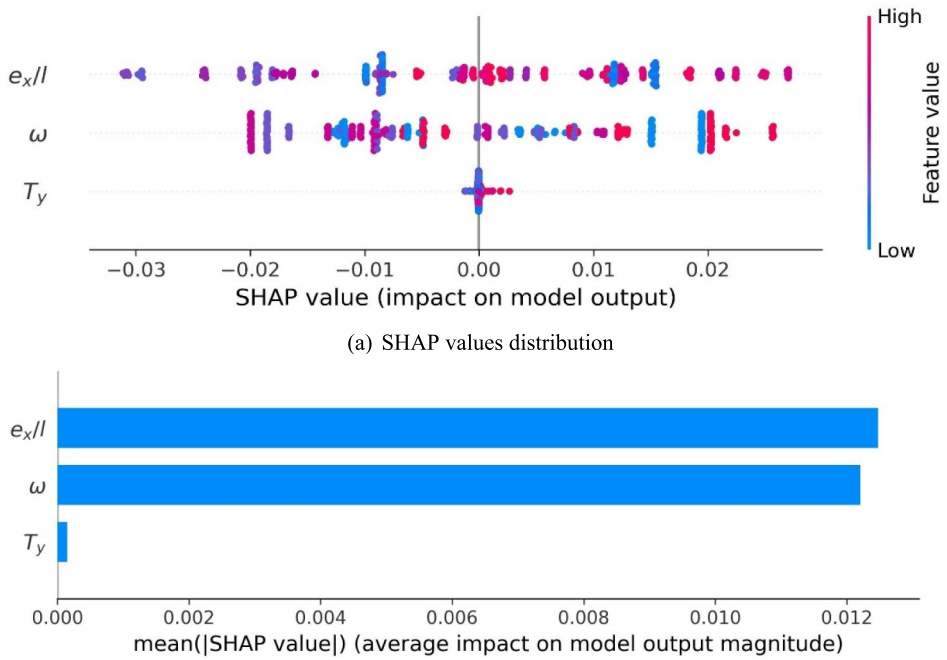

Fig. 14 Feature impact analysis on SMA performance

(a) SHAP values distribution

(b) Feature importance summary plot

damage, and ensures better serviceability during seismic events, highlighting its potential as a reliable vibration control solution.

2. GPR consistently demonstrated the highest accuracy across all response variables, achieving the lowest RMSE (0.0030) and highest R^2 (0.99) values. GPR's performance was robust, maintaining low error rates across different structural parameter combinations. The low error rates make GPR the most reliable model for predicting structural responses in asymmetric buildings equipped with SMA dampers.
3. DT also showed strong performance, particularly excelling in computational efficiency with the highest prediction speed (5700 obs/sec) and shortest training time (7.68 s). DT achieved competitive RMSE (0.0043) and R^2 (0.98) values, making it a viable option for real-time applications requiring quick and reliable predictions.
4. ANN provided a balanced performance, with moderate error rates (0.0066) and reasonable computational efficiency (3200 obs/sec). Although GPR achieved higher accuracy, ANN performed adequately across most met-

Fig. 15 SHAP dependence plots of the features on response ratio

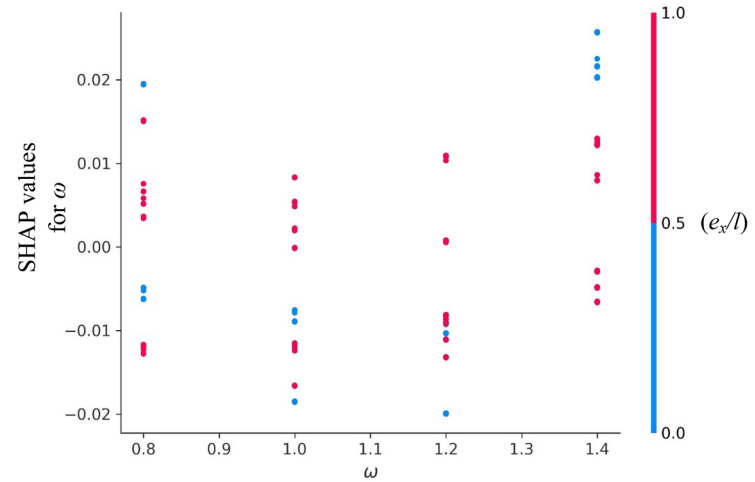

(a) SHAP value for frequency ratio (ω)

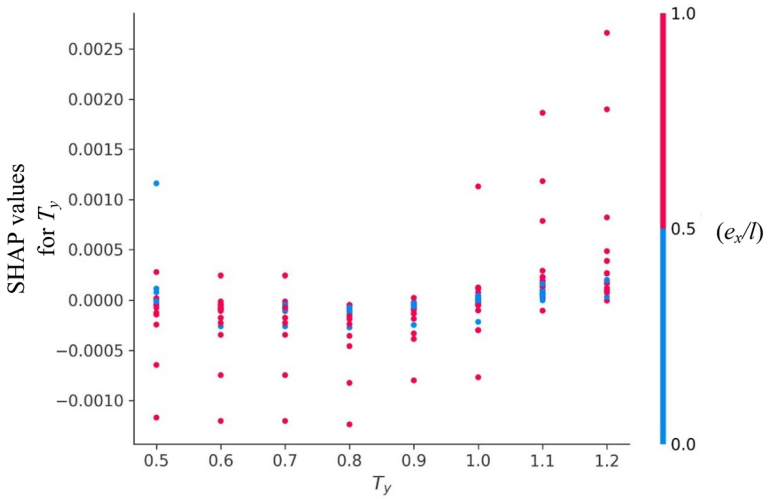

(b) SHAP value for time period (T_y)

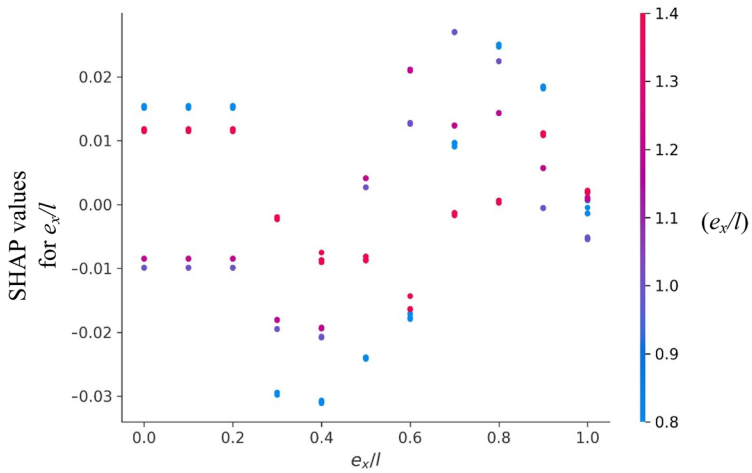

(c) SHAP value for eccentricity ratio (e_x/l)

rics, making it a suitable choice for applications that require a balance between accuracy and efficiency.

5. SVM and EBT showed mixed results in predicting and testing various parameters. However, SVM was better than EBT regarding RMSE and R^2 values (0.01 and 0.87).
6. SHAP analysis reveals that the frequency and eccentricity ratios have nearly equal effects on the response of structures equipped with SMA wire dampers. Simultaneously, the time period of the structure influences its response more than the other two parameters.

These findings suggest that GPR is the most reliable model for predicting the well-being impact of structural parameters on structural response with an SMA damper. At the same time, SVM and EBT are potential candidates for further tuning. The ANN and DT models need additional optimizations to achieve comparable levels of accuracy.

Acknowledgements The second and third authors acknowledge the Ministry of Education (MoE) of the Government of India for supporting the PhD fellowship program. The authors thank SVNIT Surat Library for providing digital access to online materials. Finally, we would like to express our gratitude to the reviewers who remained anonymous for their perspective remarks and helpful criticism, which contributed to enhancing the work.

Author contributions CRediT authorship contribution statement Anant Parghi: Conceptualization, Data curation, Formal analysis, Funding acquisition, Investigation, Methodology, Project administration, Software, Resources, Supervision, Validation, Visualization, Writing—original draft, Writing—review and editing Jay Gohel: Conceptualization, Data curation, Formal analysis, Investigation, Methodology, Software, Resources, Validation, Visualization, writing—original draft, Writing—review and editing Apurwa Rastogi: Conceptualization, Data curation, Formal analysis, Investigation, Methodology, Software, Resources, Validation, Visualization, writing—original draft, Writing—review and editing Melda Yucel: Conceptualization, Data curation, Formal analysis, Methodology, Project administration, Software, Supervision, Validation, Visualization, Writing—review and editing Cigdem Avci-Karatas: Conceptualization, Data curation, Formal analysis, Methodology, Project administration, Software, Supervision, Validation, Visualization, Writing—review and editing Snehal Mevada: Conceptualization, Data curation, Formal analysis, Methodology, Project administration, Software, Supervision, Validation, Visualization, Writing—review and editing.

Funding The authors have not disclosed any funding.

Data availability No datasets were generated or analysed during the current study.

Declarations

Conflict of interest The authors declare no conflict of interest.

References

Altabey, W. A., & Noori, M. (2022). Artificial-Intelligence-based methods for structural health monitoring. *Applied Sciences, 12*(24), 12–15. https://doi.org/10.3390/app122412726

Angarita, C., Montes, C., & Arroyo, O. (2024). Machine learning–based approach for predicting pushover curves of low-rise reinforced concrete frame buildings. *Structures, 70*(October), 107694. https://doi.org/10.1016/j.istruc.2024.107694

Breiman, L. (1996). Bagging predictors. *Machine Learning, 24*, 123–140. https://doi.org/10.3390/risks8030083

Candanedo, L. M., & Feldheim, V. (2016). Accurate occupancy detection of an office room from light, temperature, humidity and CO_2 measurements using statistical learning models. *Energy Build., 112*, 28–39. https://doi.org/10.1016/j.enbuild.2015.11.071

Chowdhury, S. (2021). Nonlinear dynamic analysis of torsionally coupled isolated structures. *Practice Periodical on Structural Design and Construction, 26*(3), 04021023. https://doi.org/10.1061/(asce)sc.1943-5576.0000591

Falahian, A., Asadi, P., Tajmir Riahi, H., & Kadkhodaei, M. (2021). An experimental study on a self-centering damper based on shape-memory alloy wires. *Mechanics Based Design of Structures and Machines, 0*(0), 1–24. https://doi.org/10.1080/15397734.2021.1939048

Feng, D. C., Liu, Z. T., Wang, X. D., Chen, Y., Chang, J. Q., Wei, D. F., & Jiang, Z. M. (2020). Machine learning-based compressive strength prediction for concrete: An adaptive boosting approach. *Construction and Building Materials, 230*, 117000. https://doi.org/10.1016/j.conbuildmat.2019.117000

Ghosh, J., Padgett, J. E., & Dueñas-Osorio, L. (2013). Surrogate modeling and failure surface visualization for efficient seismic vulnerability assessment of highway bridges. *Probabilistic Engineering Mechanics, 34*, 189–199. https://doi.org/10.1016/j.probengmech.2013.09.003

Goodfellow, I., Bengio, Y., Courville, A., & Bengio, Y. (2016). *Deep Learning*. Cambridge: MIT press.

Graesser, E. J., & Cozzarelli, F. A. (1991). Shape-memory alloys as new materials for aseismic isolation. *Journal of Engineering Mechanics, 117*(11), 2590–2608. https://doi.org/10.1061/(asce)0733-9399(1991)117:11(2590)

Jia, J., Gong, M., Zuo, Z., Wang, X., & Zhao, Y. (2025). A novel deep learning-based method for generating floor response spectra of building structures. *Engineering Structures, 322*(PA), 119058. https://doi.org/10.1016/j.engstruct.2024.119058

Kaveh, A. (2024). *Applications of artificial neural networks and machine learning in civil engineering*. Cham: Springer Cham.

Kaveh, A., & Biabani Hamedani, K. (2022). Improved arithmetic optimization algorithm. *Studies in Computational Intelligence, 1059*(November 2021), 323–362. https://doi.org/10.1007/978-3-031-13429-6_10

Kaveh, A., Fahimi Farzam, M., & Hojat Jalali, H. (2020). Statistical seismic performance assessment of tuned massdamper inerter. *Structural Control and Health Monitoring, 27*(10), e2602.

Kaveh, A., Mohammadi, S., Khadem Hosseini, O., Keyhani, A., & Kalatjari, V. R. (2015). Optimum parameters of tuned mass dampers for seismic applications using charged system search. *Iranian Journal of Science and Technology Transactions of Civil Engineering, 39*(C1), 21–40.

Kaveh, A., & Zakian, P. (2013). Optimal design of steel frames under seismic loading using two meta-heuristic algorithms. *Journal of Constructional Steel Research, 82*, 111–130. https://doi.org/10.1016/j.jcsr.2012.12.003

Kaveh, A., & Zakian, P. (2014). Seismic design optimisation of RC moment frames and dual shear wall-frame structures VIA CSS algorithm. *Asian Journal of Civil Engineering, 15*(3), 435–465.

Li, Y., Li, S., Sun, B., Liu, M., & Chen, Z. (2021). Effectiveness of a tiny tuned liquid damper on mitigating wind-induced responses of cylindrical solar tower based on elastic wind tunnel tests. *Journal of Wind Engineering and Industrial Aerodynamics, 208*(2020), 104455. https://doi.org/10.1016/j.jweia.2020.104455

Mahmoudi, S. N., & Chouinard, L. (2016). Seismic fragility assessment of highway bridges using support vector machines. *Bulletin of Earthquake Engineering, 14*(6), 1571–1587. https://doi.org/10.1007/s10518-016-9894-7

MathWorks. (2022). "MATLAB and statistics Toolbox R2022a."

Mevada, S. V., & Jangid, R. S. (2015). Seismic response of torsionally coupled building with passive and semi-active stiffness dampers. *International Journal of Advanced Structural Engineering, 7*(1), 31–48. https://doi.org/10.1007/s40091-015-0080-y

Mohammadgholipour, A., & Billah, A. H. M. M. (2023). Mechanical properties and constitutive models of shape memory alloy for structural engineering : A review. *Journal of Intelligent Material Systems and Structures, 34*, 2335–2359. https://doi.org/10.1177/1045389X231185458

Muntasir Billah, A., Rahman, J., & Zhang, Q. (2022). Shape memory alloys (SMAs) for resilient bridges: A state-of-the-art review. *Structures, 37*(May 2021), 514–527. https://doi.org/10.1016/j.istruc.2022.01.034

Pang, Y., Dang, X., & Yuan, W. (2014). An artificial neural network based method for seismic fragility analysis of highway bridges. *Advances in Structural Engineering, 17*(3), 413–428. https://doi.org/10.1260/1369-4332.17.3.413

Parghi, A., Gohel, J., Rastogi, A., & Emami, A. (2024). Seismic response of torsionally linked systems using shape memory alloy passive dampers. *Soil Dynamics and Earthquake Engineering, 183*(June), 108778. https://doi.org/10.1016/j.soildyn.2024.108778

Qian, H., Li, H., & Song, G. (2016). Experimental investigations of building structure with a superelastic shape memory alloy friction damper subject to seismic loads. *Smart Materials and Structures, 25*(12), 1–14. https://doi.org/10.1088/0964-1726/25/12/125026

Qian, H., Li, H., Song, G., & Guo, W. (2013). Recentering shape memory alloy passive damper for structural vibration control. *Mathematical Problems in Engineering*. https://doi.org/10.1155/2013/963530

Shyamsunder, L., Pandey, D. K., & Mishra, S. K. (2021). Behavior of torsionally coupled buildings isolated by super-elastic bearing subjected to earthquakes. *Journal of Building Engineering, 43*(April), 102573. https://doi.org/10.1016/j.jobe.2021.102573

Sishi, M., & Telukdarie, A. (2021). The application of decision tree regression to optimize business processes. *Proceedings of the International Conference on Industrial Engineering and Operations Management*. https://doi.org/10.46254/sa02.20210031.

Sun, Z., Feng, D.-C., Mangalathu, S., Wang, W.-J., & Su, D. (2022). Effectiveness assessment of TMDs in bridges under strong winds incorporating machine-learning techniques. *Journal of Performance of Constructed Facilities, 36*(5), 1–14. https://doi.org/10.1061/(asce)cf.1943-5509.0001746

Tabrizikahou, A., Kuczma, M., Łasecka-Plura, M., Noroozinejad Farsangi, E., Noori, M., Gardoni, P., & Li, S. (2022). Application and modelling of shape-memory alloys for structural vibration control: State-of-the-art review. *Construction and Building Materials, 342*(PB), 127975. https://doi.org/10.1016/j.conbuildmat.2022.127975

Tran-Ngoc, H., Khatir, S., Le-Xuan, T., Tran-Viet, H., De Roeck, G., Bui-Tien, T., & Wahab, M. A. (2022). Damage assessment in structures using artificial neural network working and a hybrid stochastic optimization. *Scientific Reports, 12*(1), 1–12. https://doi.org/10.1038/s41598-022-09126-8

Udaya Mohanan, K., Cho, S., & Park, B. G. (2023). Optimization of the structural complexity of artificial neural network for hardware-driven neuromorphic computing application. *Applied Intelligence, 53*(6), 6288–6306. https://doi.org/10.1007/s10489-022-03783-y

Wang, L., Zhou, Y., Nagarajaiah, S., & Shi, W. (2023). Bi-directional semi-active tuned mass damper for torsional asymmetric structural seismic response control. *Engineering Structures, 294*(August), 116744. https://doi.org/10.1016/j.engstruct.2023.116744

Wei, B., Zheng, X., Jiang, L., Lai, Z., Zhang, R., Chen, J., & Yang, Z. (2024). Seismic response prediction and fragility assessment of high-speed railway bridges using machine learning technology. *Structures, 66*(June), 106845. https://doi.org/10.1016/j.istruc.2024.106845

Wei, D., Shi, Y., Qian, H., Li, Z., & Li, H. (2025). Seismic response control of recentering steel frame with innovative SMA-high damping rubber dampers under sequential earthquakes. *Soil Dynamics and Earthquake Engineering, 188*(PB), 109033. https://doi.org/10.1016/j.soildyn.2024.109033

Yan, R., Ma, Z., Zhao, Y., & Kokogiannakis, G. (2016). A decision tree based data-driven diagnostic strategy for air handling units. *Energy and Buildings, 133*, 37–45. https://doi.org/10.1016/j.enbuild.2016.09.039

Yang, G., Wu, D., Mao, J., & Du, Y. (2024). Comprehensive resilience assessment of bridge networks using ensemble learning method. *Advances in Engineering Software, 198*(May), 103774. https://doi.org/10.1016/j.advengsoft.2024.103774

Yang, T., Wei, Y., & Zhong, J. (2023). Potential bias of conventional structural seismic fragility for bridge structures under pulse-like ground motions: Bias evaluation and strategy improvement. *Soil Dynamics and Earthquake Engineering, 166*(October 2022), 107787. https://doi.org/10.1016/j.soildyn.2023.107787

Yucel, M., Bekdaş, G., Nigdeli, S. M., & Sevgen, S. (2019). Estimation of optimum tuned mass damper parameters via machine learning. *Journal of Building Engineering, 26*(March), 100847. https://doi.org/10.1016/j.jobe.2019.100847

Zhang, Z., Bi, K., Hao, H., Sheng, P., Feng, L., & Xiao, D. (2020a). Development of a novel deformation-amplified shape memory alloy-friction damper for mitigating seismic responses of RC frame buildings. *Engineering Structures, 216*(August 2019), 110751. https://doi.org/10.1016/j.engstruct.2020.110751

Zhang, Z., Bi, K., Hao, H., Sheng, P., Feng, L., & Xiao, D. (2020b). Development of a novel deformation-amplified shape memory alloy-friction damper for mitigating seismic responses of RC frame buildings. *Engineering Structures, 216*(May), 110751. https://doi.org/10.1016/j.engstruct.2020.110751

Zhao, J., Lasternas, B., Lam, K. P., Yun, R., & Loftness, V. (2014). Occupant behavior and schedule modeling for building energy simulation through office appliance power consumption data mining. *Energy and Buildings, 82*, 341–355. https://doi.org/10.1016/j.enbuild.2014.07.033

Zhong, J., Zheng, X., Zhu, Y., & Dang, X. (2023). Resilience-based seismic design optimization of novel link beam in a double-column bridge bent using Gaussian process regression. *Bulletin of*

Earthquake Engineering, 21(13), 6121–6142. https://doi.org/10.1007/s10518-023-01762-3

Zuo, X., Key, J., Materials, C., & Province, N. J. (2008). Optimal design of shape memory alloy damper for cable vibration control. *Journal of Vibration and Control, 15*(6), 897–921. https://doi.org/10.1177/1077546308094916